

ANALYTICAL LIGHT CURVE MODELS OF SUPERLUMINOUS SUPERNOVAE: χ^2 -MINIMIZATION OF PARAMETER FITS

E. CHATZOPOULOS¹, J. CRAIG WHEELER¹, J. VINKO^{1,2}, Z. L. HORVATH², AND A. NAGY²

¹ Department of Astronomy, University of Texas at Austin, Austin, TX, USA; manolis@astro.as.utexas.edu

² Department of Optics and Quantum Electronics, University of Szeged, Hungary

Received 2013 May 2; accepted 2013 June 21; published 2013 July 29

ABSTRACT

We present fits of generalized semi-analytic supernova (SN) light curve (LC) models for a variety of power inputs including ^{56}Ni and ^{56}Co radioactive decay, magnetar spin-down, and forward and reverse shock heating due to supernova ejecta–circumstellar matter (CSM) interaction. We apply our models to the observed LCs of the H-rich superluminous supernovae (SLSN-II) SN 2006gy, SN 2006tf, SN 2008am, SN 2008es, CSS100217, the H-poor SLSN-I SN 2005ap, SCP06F6, SN 2007bi, SN 2010gx, and SN 2010kd, as well as to the interacting SN 2008iy and PTF 09uj. Our goal is to determine the dominant mechanism that powers the LCs of these extraordinary events and the physical conditions involved in each case. We also present a comparison of our semi-analytical results with recent results from numerical radiation hydrodynamics calculations in the particular case of SN 2006gy in order to explore the strengths and weaknesses of our models. We find that CS shock heating produced by ejecta–CSM interaction provides a better fit to the LCs of most of the events we examine. We discuss the possibility that collision of supernova ejecta with hydrogen-deficient CSM accounts for some of the hydrogen-deficient SLSNe (SLSN-I) and may be a plausible explanation for the explosion mechanism of SN 2007bi, the pair-instability supernova candidate. We characterize and discuss issues of parameter degeneracy.

Key words: circumstellar matter – stars: evolution – stars: mass-loss – supernovae: general

Online-only material: color figures

1. INTRODUCTION

The discovery of superluminous supernovae (SLSNe; Quimby et al. 2007, 2013; Smith et al. 2007; Gal-Yam 2012) imposed challenges to the widely used mechanism of ^{56}Ni and ^{56}Co radioactive decay diffusion (Arnett 1980, 1982, hereafter A80, A82) as the typical power input of many observed SN light curves (LCs) that do not display prominent plateaus. Attempts to fit the LCs of some SLSNe provided estimates for the mass of radioactive nickel, M_{Ni} , needed to power the peak luminosity that were close to or far exceeded corresponding estimates for the total mass of the SN ejecta (Smith et al. 2007; Chatzopoulos et al. 2011; Chatzopoulos & Wheeler 2012; see Gal-Yam 2012 for a review). The striking variety in LC shapes, peak luminosities, durations, decline rates, and spectral evolution makes the determination of a consistent physical model for the SLSNe even more challenging. Radiation hydrodynamics simulations of interactions of SN ejecta with massive circumstellar matter (CSM) shells of various power-law density profiles (Moriya et al. 2011, 2013; Ginzburg & Balberg 2012) provided important insights to the dependence of the main features of the resulting numerical LCs on the model parameters and were used to reproduce the observed LCs of some SLSNe (SN 2005ap, SN 2006gy, and SN 2010gx).

Chatzopoulos et al. (2012, hereafter CWV12) presented generalized semi-analytical models for SN LCs that take into account a variety of power inputs such as thermalized magnetar spin-down and forward and reverse shock heating due to SN ejecta–CSM interaction with some contribution from ^{56}Ni and ^{56}Co radioactive decay. CWV12 considered cases where the photosphere of the diffusion mass is either expanding homologously or stationary within an optically thick CSM. Their formalism was largely based on that of A80 and A82 to incorporate an approximation for radiative diffusion and on that

of Chevalier (1982) and Chevalier & Fransson (1994; see also Chevalier & Fransson 2001) to estimate the luminosity input from forward and reverse shocks depositing kinetic energy into the CSM and the SN ejecta, respectively. The CSM interaction plus ^{56}Ni and ^{56}Co radioactive decay LC model was successfully compared in CWV12 to some radiation hydrodynamics numerical LC models within uncertainties and was used to reproduce the LC of the SN 2006gy. The availability of easily computed analytical models allows the development of a χ^2 -minimization fitting code that can be used to fit the observed LCs of SLSNe and other interesting transients. This fitting procedure allows us to estimate the physical parameters involved and their uncertainties and to assess parameter degeneracies, a severe problem with multi-parameter models, either analytic or numerical. The resulting models give us a hint of which power input mechanism is most likely involved in these extraordinary events. This work serves as a sequel to the work of CWV12 and aims to apply fits of the models presented there to all SLSNe for which LCs were available when the work was done. The parameters derived from those fits may be used as a starting point for more accurate but computationally expensive numerical simulations in the attempt to understand the physics involved in these rare explosions.

We organize the paper as follows. In Section 2 we summarize the analytical LC models that were presented by CWV12 and used in this work to fit observed LCs. We also present comparisons of our semi-analytic SN ejecta–CSM interaction model from CWV12 with numerical LC models of SN 2006gy. In Section 3 we describe our observational sample of SLSNe and SNe IIn and in Section 4 the fitting method that was incorporated in our χ^2 -minimization fitting code and present an analysis of how it calculates uncertainties and parameter degeneracy related to the large parameter space. We also present model fits to all events in our sample. Finally, in Section 5 we summarize our conclusions.

2. SIMPLE MODELS FOR SLSNe LIGHT CURVES

The analytical SN LC models that we use to fit observed SLSN LCs are presented in detail in CWV12. Here, we give a review of the models and of their physical assumptions. The derivation of those models was largely based on the methods discussed in A80 and A82 making the assumptions of homologous expansion for the SN ejecta, centrally located power input source, radiation pressure being dominant, and separability of the spatial and temporal behavior. In the generalized solutions presented in CWV12 we have relaxed the criterion for homologous expansion of the ejecta and also considered cases for large initial radius as may be the case for the progenitors of some SLSNe, as well as cases where the photosphere is stationary within an optically thick CSM envelope, as may be the case for luminous interacting SNe IIn. The CSM interaction models include bolometric LCs for both optically thick and optically thin situations, as appropriate. The generalized solutions are presented for a variety of power input mechanisms, including those that have been proposed in the past.

The first power input mechanism considered is the radioactive decay of ^{56}Ni and ^{56}Co (hereafter the RD model) that leads to the deposition of energetic gamma rays that are assumed to thermalize in the homologously expanding SN ejecta. As presented in CWV12, the generalized LC model in this case has the following form:

$$L(t) = \frac{2M_{\text{Ni}}}{t_d} e^{-[x^2+2wx]} \{(\epsilon_{\text{Ni}} - \epsilon_{\text{Co}}) \times \int_0^x (w+x') e^{[x'^2+2wx']} e^{-t_d/t_{\text{Ni}}x'} t_d dx' + \epsilon_{\text{Co}} \int_0^x (w+x') e^{[x'^2+2wx']} \times e^{-t_d/t_{\text{Co}}x'} t_d dx'\} \cdot (1 - e^{-At^{-2}}), \quad (1)$$

where $L(t)$ is the output luminosity in erg s^{-1} , t is the time in days relative to the time of explosion t_{ini} (see the Appendix), M_{Ni} is the initial nickel mass, t_d is the effective LC timescale (the mean of the hydrodynamical and diffusion timescales as defined by A80), $x = t/t_d$ is the dimensionless time variable, R_0 is the initial radius of the progenitor, v is the expansion velocity of the ejecta, $w = R_0/(vt_d)$ is the ratio of the hydrodynamical and the LC timescales, $t_{\text{Ni}} = 8.8$ days, $t_{\text{Co}} = 111.3$ days are the timescales of Ni- and Co-decay, and $\epsilon_{\text{Ni}} = 3.9 \times 10^{10} \text{ erg s}^{-1} \text{ g}^{-1}$ and $\epsilon_{\text{Co}} = 6.8 \times 10^9 \text{ erg s}^{-1} \text{ g}^{-1}$ are the specific energy generation rates due to Ni and Co decays, respectively (Nadyozhin 1994; Valenti et al. 2008). The factor $(1 - e^{-At^{-2}})$ accounts for the gamma-ray leakage, where large A means that practically all gamma rays and positrons are trapped. The gamma-ray optical depth of the ejecta is taken to be $\tau_\gamma = \kappa_\gamma \rho R = At^{-2}$, where κ_γ is the gamma-ray opacity of the SN ejecta (typically $\sim 0.03 \text{ cm}^2 \text{ g}^{-1}$; Colgate et al. 1980). Taking into account that $R_0/vt_d \ll 1$ for all SNe considered in this paper, the application of Equation (1) is greatly simplified. Thus, the fitting parameters for this model are M_{Ni} , t_d , and A , since reasonable assumptions can be made for v based on observations.

Another input that has recently been used to explain the LCs of some SLSNe such as SN 2008es and SN 2007bi is that of the energy released by the spin-down of a young magnetar located in the center of the SN ejecta (hereafter the ‘‘MAG’’ model; Ostriker & Gunn 1971; Arnett & Fu 1989; Maeda et al. 2007; Kasen & Bildsten 2010; Woosley 2010). The LC of an SN

powered by such input is given by the following formula:

$$L(t) = \frac{2E_p}{t_p} e^{-[x^2+wx]} \int_0^x e^{[x'^2+wx']} \frac{x'+w}{(1+yx')^2} dx', \quad (2)$$

where $x = t/t_d$ and $y = t_d/t_p$ with t_d again being an ‘‘effective’’ diffusion time, E_p the initial magnetar rotational energy, and t_p = the characteristic timescale for spin-down that depends on the strength of the magnetic field. For a fiducial moment of inertia (10^{45} g cm^2), the initial period of the magnetar in units of 10 ms is given by $P_{10} = (2 \times 10^{50} \text{ erg s}^{-1}/E_p)^{0.5}$. The dipole magnetic field of the magnetar can be estimated from P_{10} and t_p as $B_{14} = (1.3 P_{10}^2/t_{p,\text{yr}})^{0.5}$, where B_{14} is the magnetic field in units of 10^{14} G and $t_{p,\text{yr}}$ is the characteristic timescale for spin-down in units of years. Therefore, for the MAG model the fitting parameters are E_p , t_p , R_0 , and t_d . We note that this model assumes that the input from the pulsar is thermalized in the ejecta. Simulations of this process show that the energy may not thermalize, but be ejected as magnetohydrodynamic (MHD) jets (Bucciantini et al. 2006), thus compromising the mechanism as a model for SLSNe.

For both the RD and the MAG models, the SN ejecta mass, M_{ej} , is given by the following equation:

$$M_{\text{ej}} = \frac{3}{10} \frac{\beta c}{\kappa} v t_d^2, \quad (3)$$

where M_{ej} is the mass of the SN ejecta, β is an integration constant equal to about 13.8, and c is the speed of light. The value of M_{ej} for a particular SN determined by its LC is uncertain because of the uncertainties associated with κ . For the purposes of this work we will adopt the Thomson electron scattering opacity for fully ionized solar metallicity material ($\kappa \sim 0.33 \text{ cm}^2 \text{ g}^{-1}$). We also adopt as a fiducial value for the expansion velocity $v = 10,000 \text{ km s}^{-1}$ for the estimates presented in the tables. The uncertainty of M_{ej} has an important effect on the criterion $M_{\text{Ni}} < M_{\text{ej}}$ that serves as a consistency check for the RD model.

Another power input that is accepted as being the dominant one in the case of some SLSNe and SNe IIn is that of shock heating. Some SN progenitors are embedded within dense CSM environments that are formed via continuous or sporadic mass loss. When the SN explosion occurs, the SN ejecta violently interact with the CSM, producing a double shock structure composed of a forward shock moving in the CSM and a reverse shock moving back into the SN ejecta. Both the forward and the reverse shocks deposit kinetic energy into the material which is then radiatively released powering the LCs of these events. The physics of SN ejecta–CSM interaction is described in the works of Chevalier (1982) and Chevalier & Fransson (1994). Simplified models based on this mechanism have recently been considered as a power source for some SNe IIn (Wood-Vasey et al. 2004; Ofek et al. 2010; Chevalier & Irwin 2011). The X-ray flux produced by CSM interaction-powered events has also been studied in different contexts (CWV12; Chevalier & Irwin 2012; Svirski et al. 2012; Ofek et al. 2013; Pan et al. 2013; Chevalier 2013). In addition, a few numerical radiation hydrodynamics simulations have been performed yielding broadband model LCs with the purpose of reproducing the LCs of some events (Chugai et al. 2004; Moriya et al. 2011, 2013). CWV12 presented an analytical LC model that incorporates the effects of forward and reverse shock deposited energy with those of diffusion through an optically thick CSM under the assumption that the shocks are deep within the photosphere so that the

typical shock crossing timescale is larger than the effective radiation diffusion timescale. The models of CWV12 are in the same regime discussed by Chevalier & Irwin (2011), but their generalized model for diffusion spans both cases examined by Chevalier & Irwin ($R_d < R_{\text{CSM}}$ and $R_d > R_{\text{CSM}}$, with R_d defined to be the distance from which radiation can escape from the forward shock). CWV12 also presented a hybrid version of this model where the effects of energy deposition by the radioactive decays of ^{56}Ni and ^{56}Co are also considered (hereafter the CSM+RD model), given by the following expression:

$$\begin{aligned}
L(t) = & \frac{1}{t_0} e^{-\frac{t}{t_0}} \int_0^t e^{\frac{t'}{t_0}} \left[\frac{2\pi}{(n-s)^3} g^n \frac{\delta^{3-n}}{n-s} q^{\frac{n-s}{n-s}} (n-3)^2 \right. \\
& \times (n-5) \beta_F^{5-s} A^{\frac{5-s}{n-s}} (t' + t_i)^\gamma \cdot \theta(t_{\text{FS,BO}} - t') \\
& + 2\pi \left(\frac{A g^n}{q} \right)^{\frac{5-n}{n-s}} \beta_R^{5-n} g^n \\
& \times \left(\frac{3-s}{n-s} \right)^3 (t' + t_i)^\gamma \cdot \theta(t_{\text{RS,*}} - t') \Big] dt' \\
& + \frac{M_{\text{Ni}}}{t'_0} e^{-\frac{t}{t'_0}} \int_0^t e^{\frac{t'}{t'_0}} [(\epsilon_{\text{Ni}} - \epsilon_{\text{Co}}) e^{-\frac{t'}{t'_{\text{Ni}}}} + \epsilon_{\text{Co}} e^{-\frac{t'}{t'_{\text{Co}}}}] dt',
\end{aligned} \tag{4}$$

where t_0 and t'_0 correspond to the diffusion timescales through the mass of the optically thick part of the CSM, $M_{\text{CSM,th}}$, and the sum of the mass of the ejecta and the optically thick part of the CSM, $M_{\text{ej}} + M_{\text{CSM,th}}$, respectively, s is the power-law exponent for the CSM density profile, $q = \rho_{\text{CSM},1} r_1^s$, where $\rho_{\text{CSM},1}$ is the density of the CSM shell at $r = r_1$ (we use as a fiducial value $r_1 = R_p$, where R_p is the radius of the progenitor star, thus we set the density scale of the CSM, $\rho_{\text{CSM},1}$, immediately outside the stellar envelope), g^n is a scaling parameter for the ejecta density profile, $g^n = 1/(4\pi(\delta - n)[2(5 - \delta)(n - 5)E_{\text{SN}}]^{(n-3)/2}/[(3 - \delta)(n - 3)M_{\text{ej}}]^{(n-5)/2}$, where n is the power-law exponent of the outer component, and δ is the slope of the inner density profile of the ejecta (values of $\delta = 0, 2$ are typical), E_{SN} is the total SN energy, $\gamma = (2n + 6s - ns - 15)/(n - s)$, β_F , β_R , and A are constants that depend on the values of n and s and, for a variety of values, are given in Table 1 of Chevalier (1982), $\theta(t_{\text{FS,*}} - t)$ and $\theta(t_{\text{RS,*}} - t)$ denote the Heaviside step functions that control the termination of the forward and reverse shock, respectively ($t_{\text{FS,*}}$ and $t_{\text{RS,*}}$ are the termination timescales for the two shocks), and $t_i \simeq R_p/v_{\text{SN}}$ is the initial time of the CSM interaction that sets the initial value for the luminosity produced by shocks where $v_{\text{SN}} = [10(n - 5)E_{\text{SN}}/3(n - 3)M_{\text{ej}}]^{1/2}/x_0$ is the characteristic velocity of the SN ejecta and $x_0 = r_0(t)/R_{\text{SN}}(t)$ is the dimensionless radius of the break in the SN ejecta density profile from the inner flat component (described by δ) to the outer, steeper component (described by n), which is at radius $r_0(t)$. This hybrid CSM+RD model can be easily turned into a pure CSM interaction LC model by setting $M_{\text{Ni}} = 0$. Moriya et al. (2013) noted that in the case of SN 2006gy CSM interaction is the dominant source of the input energy with any additional energy due to ^{56}Ni and ^{56}Co decays found to be negligible and not to contribute to any of the main features of the resulting LC.

The forward and reverse shock termination timescales are given by

$$t_{\text{FS,*}} = \left| \frac{3-s}{4\pi\beta_F^{3-s}} q^{\frac{3-n}{n-s}} (A g^n)^{\frac{3-s}{n-s}} \right|^\xi M_{\text{CSM}}^\xi, \tag{5}$$

where $\xi = (n - s)/((n - 3)(3 - s))$, and

$$t_{\text{RS,*}} = \left[\frac{v_{\text{SN}}}{\beta_R (A g^n / q)^{\frac{1}{n-s}}} \left(1 - \frac{(3-n)M_{\text{ej}}}{4\pi v_{\text{SN}}^{3-n} g^n} \right)^{\frac{1}{3-n}} \right]^{\frac{n-s}{3-n}}, \tag{6}$$

respectively. A simplifying and convenient assumption of our model is that it does not take into account the movement of the shocks in the involved diffusion masses (SN ejecta and CSM), which has a direct effect on the LC diffusion timescale. In reality, the forward shock will propagate toward the photosphere within the optically thick CSM envelope, therefore having an ever-decreasing diffusion time that will lead to a faster evolution for the LC. This caveat was discussed in CWV12 and underlined in radiation hydrodynamic models recently presented by Moriya et al. (2013). In Section 2.1 we present a comparison between our CSM+RD model LC for SN 2006gy and the numerical model obtained by Moriya et al. (2013) using the same parameters that they used in one of their best-fitting models.

The large parameter space associated with SN ejecta–CSM interaction is reflected by the large number of fitting parameters in this hybrid CSM+RD model: parameters associated with the nature of the progenitor star (δ , n , v_{SN} , R_p , M_{ej} , M_{Ni}) and parameters associated with the nature of the CSM (M_{CSM} , s , $\rho_{\text{CSM},1}$). Since we fix δ , n , and s for the model fits presented here, we have a total of six fitting parameters, making fits to observed SN LCs hard to constrain. The main fitting parameters can be used to derive other physical quantities that give constraints on the configuration of the CSM envelope implied by a certain fit, in particular the energy of the supernova explosion $E_{\text{SN}} = [3(n - 3)/(2(5 - \delta)(n - 5))]M_{\text{ej}}(x_0 v_{\text{SN}})^2$ (where x_0 is the dimensionless radius where the supernova ejecta density profile breaks from a flat to a steep power law), the radius of the photosphere within the CSM envelope, R_{ph} , the total radius of the CSM shell, R_{CSM} , and the optical depth of the CSM, τ_{CSM} . Due to the large parameter space associated with the hybrid CSM+RD LC model, a simplified version of shock heating input, which considers the input to be a “top-hat” function of time, is also presented in CWV12 and can be used for some illustrative fits (hereafter the “TH” model). In this model, constant shock energy input E_{sh} is injected in a diffusion mass for a time, t_{sh} , and then shuts off. For this model, the output LC in the case of fixed photospheric radius is given by

$$L(t) = \begin{cases} \frac{E_{\text{sh}}}{t_{\text{sh}}} [1 - e^{-t/t_{\text{sh}}}], & t < t_{\text{sh}}, \\ \frac{E_{\text{sh}}}{t_{\text{sh}}} e^{-t/t_{\text{sh}}} [e^{t_{\text{sh}}/t_{\text{sh}}} - 1], & t > t_{\text{sh}} \end{cases}. \tag{7}$$

2.1. SN 2006gy: A Comparison with Results by Radiation Hydrodynamics Calculations

In CWV12 we presented an indicative fit of the hybrid CSM+RD model to the observed KAIT LC of the archetypical superluminous SN 2006gy (Smith et al. 2007), and provided a discussion of the event in the context of a variety of LC powering mechanisms. Moriya et al. (2013) presented one-dimensional (1D) radiation hydrodynamics simulations of SN ejecta with CSM envelopes with power-law density profiles for several power-law indices ($s = 0, 2$ and 5) performed with the code STELLA (Blinnikov & Bartunov 1993). Moriya et al. (2013) also present a comparison of their numerical LC with our analytical model using the same parameters as presented in CWV12 and note several discrepancies between the two (their Section 6.4 and Figure 14). We therefore find it interesting to

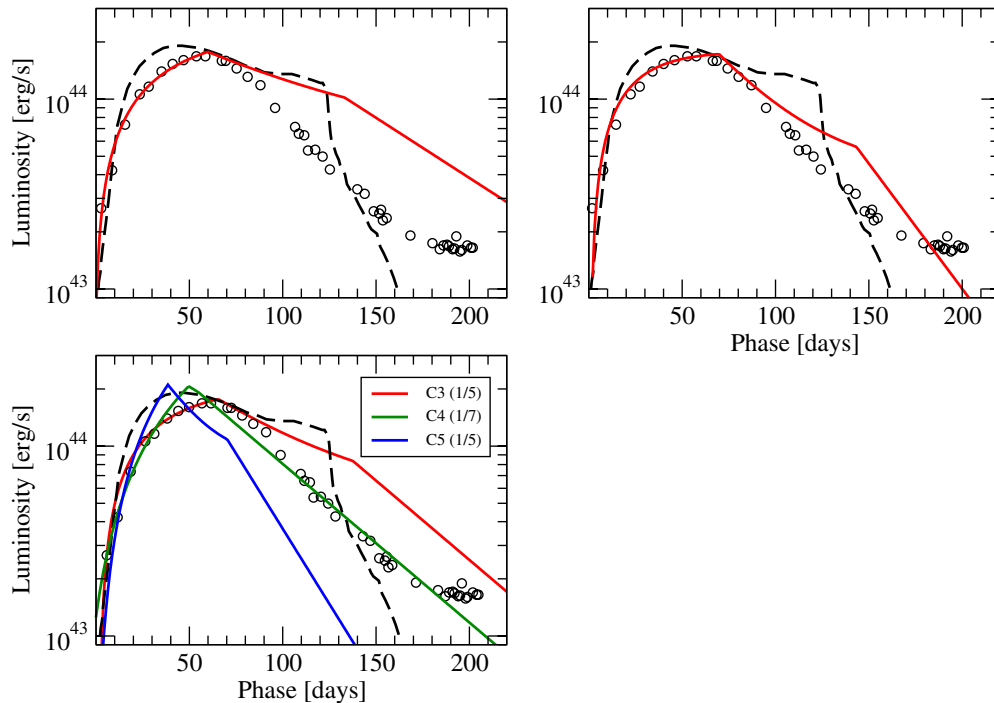


Figure 1. Comparison of the LCs from the hybrid CSM+RD model with the observed KAIT photometry of SN 2006gy. The model parameters are listed in Table 1. The dashed curve shows the model LC computed with the same parameters as model F1 of Moriya et al. (2013) scaled to fit the observed maximum luminosity. Our additional models are plotted as colored continuous curves: model C1 (upper left panel), model C2 (upper right panel), and models C3, C4, and C5 (lower left panel; the models are scaled to the observations with a factor indicated in the legends). Model C4 provides a reasonable fit to the observations.

(A color version of this figure is available in the online journal.)

further compare our approximate models with their numerical results for SN 2006gy in order to better assess the limitations and weaknesses due to the assumptions made for the analytical models.

To do so, we pick the parameters given for model F1 of Moriya et al. (2013), which is one of their models that best reproduces the observed LC of SN 2006gy. For this model we have: $E_{\text{SN}} = 10^{52}$ erg, $M_{\text{ej}} = 20 M_{\odot}$, $M_{\text{CSM}} = 15 M_{\odot}$, $\delta = 1$, $n = 7$, $s = 0$, and $M_{\text{Ni}} = 0$. The outer radius of the CSM is $R_{\text{CSM},o} = 1.1 \times 10^{16}$ cm and the inner radius $R_{\text{CSM},i} = 5 \times 10^{15}$ cm, giving a thickness of the CSM shell of $\Delta R = 6 \times 10^{15}$ cm. While our radii are different, our ΔR is the same as Moriya et al. (2013). Thomson scattering is the dominant source of opacity in the CSM beyond the forward shock in the simulations of Moriya et al. (2013) and has the value $\kappa = 0.34 \text{ cm}^2 \text{ s}^{-1}$ for a solar mixture ($X = 0.7$), but it is calculated self-consistently in the radiation hydrodynamics calculations. The radius of the progenitor star is not a parameter considered in the simulations of Moriya et al. (2013), who start their simulations by considering freely expanding SN ejecta with a density profile that is described by Chevalier & Soker (1989). It is likely that the progenitors of those SNe are large, therefore we adopt R_p to be in the range $\sim 10^{13}$ – 10^{14} cm consistent with either blue supergiant stars or red supergiant stars. Moriya et al. (2013) consider the collision between the SN ejecta and the CSM shell to be inelastic, therefore associated with an energy conversion efficiency. For the F1 model, it is determined that only 29% of the total SN energy is converted to radiation yielding $E_{\text{rad}} = 2.9 \times 10^{51}$ erg. In our semi-analytical hybrid CSM+RD model the conversion efficiency of the shock kinetic energy to radiation is assumed to be 100%. Additionally, in order to take into account multi-dimensional effects such as Raleigh–Taylor instabilities (present in the dense CSM shell)

Table 1
Summary of the Parameters of the CSM+RD Models Presented in Figure 1 and Compared to the F1 Model of Moriya et al. (2013)

Parameter	C1	C2	C3	C4	C5	F1
s	0	0	0	0	0	0
κ ($\text{cm}^2 \text{ g}^{-1}$)	0.2	0.09	0.33	0.33	0.33	0.34
R_{CSM} (10^{15} cm)	2.4	2.0	6.0	6.0	6.0	6.0
M_{CSM} (M_{\odot})	15	15	15	15	5.0	15
n	7	7	7	12	12	7
E_{SN} (10^{51} erg)	2.2	1.7	10	10	10	10
M_{ej} (M_{\odot})	20	20	20	20	20	20
R_p (10^{13} cm)	1.0	0.9	10	10	10	...

in 1D calculations, Moriya et al. (2013) consider a “smearing” parameter B_q . Taking these model variations into consideration together with the uncertainty associated when converting the observed magnitudes to bolometric luminosities induces a general uncertainty in the value of E_{SN} . Moriya et al. (2013) estimate E_{SN} to be greater than 4×10^{51} erg for SN 2006gy.

Keeping in mind the above-mentioned uncertainties in the values of E_{SN} , R_p , and, κ we present several variations of the model F1 LC in Figure 1 and Table 1 as calculated with our semi-analytical CSM interaction model presented by Equation (4) in order to explore how closely our models agree with theirs for similar parameter choices. In the top left panel of Figure 1 we present model C1 with $E_{\text{SN}} = 2.2 \times 10^{51}$ erg, $R_p = 10^{13}$ cm, $R_{\text{CSM}} = 2.4 \times 10^{15}$ cm, and $\kappa = 0.2 \text{ cm}^2 \text{ s}^{-1}$. This value of κ is suitable for a hydrogen-poor CSM. Although this is not the case for SN 2006gy, this choice allows for the fact that one of the assumptions of the semi-analytical model is that the energy deposition from the forward and reverse shocks takes place at a constant radius deep within the CSM while,

in reality, the double-shock structure moves outward in radius reaching smaller and smaller optical depths and resulting in ever-decreasing diffusion timescales. As a result, a way to account for this diffusion timescale decrease in our model is to assume a smaller “effective” optical opacity.

It can be seen in Figure 1 that this model represents well the rising part and the peak luminosity of the LC of SN 2006gy, but has difficulty fitting the post-maximum decline. A much better result is obtained for an even smaller choice for κ ($0.09 \text{ cm}^2 \text{ s}^{-1}$) and for $E_{\text{SN}} = 1.7 \times 10^{51} \text{ erg}$, $R_p = 0.9 \times 10^{13} \text{ cm}$, and $R_{\text{CSM}} = 2 \times 10^{15} \text{ cm}$ (upper right panel, model C2). In the lower left panel we present three more variations of the Moriya et al. (2013) F1 model that use the same $E_{\text{SN}} = 10^{52} \text{ erg}$, $R_p = 10^{14} \text{ cm}$, and $\kappa = 0.33 \text{ cm}^2 \text{ s}^{-1}$, but with varying slope of the ejecta density profile and the mass of the CSM ($n = 7$, $M_{\text{CSM}} = 15 M_{\odot}$ for the red curve fitted in the open circles (model C3); $n = 12$, $M_{\text{CSM}} = 15 M_{\odot}$ for the green curve fitted in the open squares (model C4); $n = 12$, $M_{\text{CSM}} = 5 M_{\odot}$ for the blue curve fitted in the open triangles (model C5)). The open circles, squares, and triangles represent the same SN 2006gy LC data moved in the time axis by different constant values (days) in order to best match the corresponding models. We note that for these models we had to scale down the resulting luminosities by factors of 5–7 in order to fit the SN 2006gy data. As we noted above, this uncertainty results from the fact that we assume 100% conversion efficiency from kinetic energy of the shocks to radiation in our model (leading to more luminous outputs). Decreasing the luminosity is roughly equivalent to decreasing the conversion efficiency. Also, we recall that our LC of SN 2006gy is constructed assuming a zero BC for the observed magnitudes. The BC for such a complex luminous SN IIn is expected to be large and to vary with time as the LC evolves, especially due to the fact that the bulk of the shock deposited energy is emitted at short wavelengths (UV and soft X-rays) particularly in early epochs (Chevalier & Fransson 1994). It can be seen that model C4 best reproduces the LC of SN 2006gy. This model uses the same parameters as the F1 model of Moriya et al. (2013) with a different choice for n (12 instead of 7 that corresponds better to the SN ejecta density profile slope for a red supergiant progenitor star) and the luminosity scale-down by a factor of ~ 7 .

The comparisons of the semi-analytical versions of the F1 model of Moriya et al. (2013) with the observed LC of SN 2006gy presented above lead to the main conclusion that, within the uncertainties associated with the semi-analytic model and its simplifying and convenient assumptions, it can be a useful tool to provide estimates of the physical parameters associated with SLSN-II. The considerable differences between the first version of our hybrid CSM+RD model for SN 2006gy that we presented in CWV12 and the numerical LC of Moriya et al. (2013) for the same parameters are partially attributable to the large parameter space associated with SN ejecta–CSM interaction that makes it hard to find an “absolute” minimum value for χ^2 representing the true best fit to the LC data. It is possible that there are several combinations of the semi-analytic CSM interaction model parameters that produce fits of similar quality but for which more accurate, numerical LCs might not be good representations of the observed LC. This was the case for the initial CSM+RD model we presented for the LC of SN 2006gy in CWV12. For this reason we think it is useful to use the semi-analytical models in order to obtain a number of good fits corresponding to χ^2 minima and then to use those fits as starting points to perform more computationally expensive and

physically self-consistent numerical radiation hydrodynamics simulations that will certainly clarify which parameter choice best matches observed LC data.

3. THE OBSERVATIONAL SAMPLE OF SLSNe

In this section we give a brief description of the SNe studied. We use the available photometric observations of recently discovered SLSNe that are of spectral type IIn (SN 2006gy, 2006tf, 2008am, 2008es, and CSS100217), as well as those in the hydrogen-deficient category defined by Quimby et al. (2011; SN 2005ap, SCP06F6, 2010gx) and those that are candidates to be pair-instability supernovae (PISNe) and similar events (SN 2007bi, 2010kd). A recent review by Gal-Yam (2012) classifies SLSNe in a similar manner, referring to hydrogen-rich events as SLSN-II and to hydrogen-poor events as SLSN-I, but also defines the SLSN-R category for events that are thought to explode due to the pair-instability mechanism and hypothesized to be powered by large amounts of radioactive ^{56}Ni (SN 2007bi). In our classification scheme, the SLSN-I category includes the SLSN-R events. We also fit two recent Type IIn SNe (2008iy and PTF 09uj) that are not SLSNe, but their observed spectra and LCs are governed by strong CSM interaction. The reason for their inclusion in the present paper is that they can serve as test cases for our simplified CSM interaction model described in Section 2. A summary of the basic characteristics of the sample of SNe studied in this work is presented in Table 2. The blackbody temperatures, T_{BB} , are estimated using the observed peak pseudo-bolometric luminosities and assuming homologous expansion up to the time of maximum light, therefore using the radius $R_{\text{SN,max}} = v_{\text{SN}} t_{\text{rise}}$, where v_{SN} is the estimated photospheric velocity of each event as derived from spectroscopic observations. Note that the T_{BB} values are similar between SLSN-I and SLSN-II (10,000–20,000 K).

3.1. Normal SNe with Strong CSM Interaction

3.1.1. SN 2008iy

The Catalina Real-Time Transient Survey (CRTS; Drake et al. 2009) discovered SN IIn 2008iy. SN 2008iy was not an SLSN, but had the longest rise time to maximum luminosity known in the history of SNe (~ 400 days; Miller et al. 2010).

Miller et al. (2010) present an extensive photometric study of SN 2008iy in the IR (PAIRITEL), optical (Nickel and DS), and UV (*Swift*) bands. Studying the pre-explosion CRTS frames, Miller et al. (2010) accept the explosion date to be $\text{MJD}_{\text{expl}} = 54,356$, and allow for an uncertainty of approximately 50 days prior to that. Keck LRIS and Kast Lick-3m Shane telescope spectra confirmed SN 2008iy as a classic SN IIn with strong intermediate-width H and He emission features. The characteristic velocity implied by the FWHM of the $\text{H}\alpha$ line is $\sim 5000 \text{ km s}^{-1}$. Miller et al. (2010) marginally detect P Cygni profiles associated with late-time (~ 91 days after discovery) $\text{H}\alpha$ features that give a hint of photospheric expansion associated with SN 2008iy. The redshift of SN 2008iy is $z = 0.0411$. The extremely long rise time of SN 2008iy prompted Miller et al. (2010) to adopt a scenario of extensive CSM interaction as a natural explanation for this event. They specifically discussed a model of interaction with CSM clumps (Chugai & Danziger 1994) in which the number density of the clumps increases over a radius of $\sim 1.7 \times 10^{16} \text{ cm}$ from the progenitor.

To produce the pseudo-bolometric LC of the event, we convert the available DS and Nickel *I*-band magnitudes of SN 2008iy to bolometric luminosities, assuming $\text{BC} = 0$. Note that the

Table 2
Basic Data for the Studied SLSNe

SN	Type	z	t_{exp} (MJD)	L_{peak} (10^{43} erg s $^{-1}$)	T_{BB} (10^4 K)	Reference
SN2008iy	IIn	0.041	54356	1.12	1.6	Miller et al. (2010)
PTF09uj	IIn	0.065	55000	1.41	1.7	Ofek et al. (2010)
SN2006gy	SLSN-II	0.019	53967	21.40	1.2	Smith et al. (2007)
SN2006tf	SLSN-II	0.074	54050	5.20	0.8	Smith et al. (2008)
SN2008am	SLSN-II	0.234	54439	26.73	1.2	Chatzopoulos et al. (2011)
SN2008es	SLSN-II	0.202	54574	31.04	1.4	Gezari et al. (2009)
CSS100217	SLSN-II	0.147	55160	42.02	1.6	Drake et al. (2011)
SN2005ap	SLSN-I	0.283	53430	37.02	2.0	Quimby et al. (2007)
SCP06F6	SLSN-I	1.189	53772	23.72	1.4	Barbary et al. (2009)
SN2007bi	SLSN-I	0.129	54089	11.10	1.2	Gal-Yam et al. (2009)
SN2010gx	SLSN-I	0.230	55260	9.71	1.5	Pastorello et al. (2010)
SN2010kd	SLSN-I	0.101	55483	8.20	1.4	Vinko et al. (2012)

DS band is similar to the Sloan Digital Sky Survey (SDSS) i' band, so also in good agreement with Nickel I band. Using only single-band magnitudes to estimate the bolometric LC is a very approximate approach, but our intention is to get only order-of-magnitude estimates of the basic physical parameters that affect the LC the most, without attempting a detailed fine-tuned analysis and modeling of a particular object.

3.1.2. PTF 09uj

The Palomar Transient Factory (PTF) reported the discovery of the transient PTF 09uj that was identified as a Type IIn event (Ofek et al. 2010). This object is not an SLSN but has been modeled with CSM interaction, so we include it in our own study. PTF 09uj was discovered during its rise to maximum light by the Oschin 48-inch Schmidt telescope (P48) at Palomar Observatory. Pre-explosion images by *Galaxy Evolution Explorer* constrained the explosion time of the SN to be $\text{MJD}_{\text{expl}} = 55,000$, which was used for the LCs presented by Ofek et al. (2010). P48 R -band and P60 r -band follow-up photometry of the event was presented in the same work. A Lick spectrum obtained around peak luminosity revealed emission lines of H and He, typical for Type IIn events. Only a hint of P Cygni absorption associated with $\text{H}\alpha$ was detected (Ofek et al. 2010). The Lick spectrum was also used to determine the redshift of the SN ($z = 0.065$). Ofek et al. (2010) interpreted PTF 09uj with a model of ejecta–CSM interaction, where the CSM is a dense wind ($s = 2$). The same study derived the characteristic values $\dot{M} = 0.1 M_{\odot} \text{ yr}^{-1}$ and $v_w = 100 \text{ km s}^{-1}$ for the mass-loss rate and the velocity of the wind of the progenitor star. Under these assumptions the whole LC of this event is powered by CS shock breakout from the optically thick part of the wind. To derive these estimates, Ofek et al. (2010) took the diffusion time to be equal to the time of shock breakout and assumed a value $v_{\text{sh}} = 10,000 \text{ km s}^{-1}$ as the typical velocity of the CS shock, which we will also adopt for the purposes of our study. As above, we converted the P48 R - and P60 r -band LC of PTF 09uj to produce a pseudo-bolometric LC assuming $\text{BC} = 0$.

3.2. Hydrogen-rich Superluminous Events (SLSN-II)

3.2.1. SN 2006gy

The archetypical SLSN IIn SN 2006gy was discovered by the Texas Supernova Search (TSS) project and first presented by Smith et al. (2007). At the observed redshift of SN 2006gy,

$z = 0.074$, the absolute visual peak magnitude of the event reached ~ -22 mag, making it one of the brightest explosions ever discovered. A rich database of optical spectra was obtained for SN 2006gy (Smith et al. 2007, 2008, 2010) that provides an extensive record of its spectral evolution. SN 2006gy showed strong Balmer emission features with their narrow components associated with P Cygni absorption indicative of photospheric (or CSM) expansion. The $\text{H}\alpha$ line profile evolved throughout the course of the LC of SN 2006gy showing an evolution that is marked by three phases described in Smith et al. (2010). The FWHM of H, around maximum light, reveals characteristic velocities of $\sim 4000 \text{ km s}^{-1}$. Here, we consider the KAIT LC of SN 2006gy presented in Smith et al. (2007) converted to a pseudo-bolometric LC assuming bolometric correction $\text{BC} = 0$. We also adopt $E(B - V) = 0.72$ mag, yielding R -band extinction $A_R = 1.68$ mag, also in accordance with Smith et al. (2007). It has been suggested (Smith et al. 2007, 2010; Smith & McCray 2007) that the progenitor of SN 2006gy was most likely a luminous blue variable (LBV)-type star that suffered extreme mass loss prior to its death. In the same framework, upon explosion the SN ejecta violently collided with the LBV nebula, producing the observed high luminosity via shock energy deposition. A similar model of interaction between multiply ejected shells in the context of a pulsational pair instability supernova (PPISN) has also been suggested (Heger & Woosley 2002; Woosley et al. 2007).

3.2.2. SN 2006tf

SN 2006tf was a strongly interacting Type IIn SN discovered by the TSS project (Smith et al. 2008). The B -, V -, R -, and I -band LC of SN 2006tf was constructed using observations from the KAIT telescope. The SN was discovered after peak luminosity so the explosion date of SN 2006tf remains unknown. This will have an impact on the parameters of the models that we attempt to fit below. As an initial value for the explosion date, we adopt $\text{MJD}_{\text{expl}} = 54,050$, which is 50 days prior to the first photometric observation by the KAIT R band and within the range proposed by Smith et al. (2008). The spectra of SN 2006tf were characteristic of the Type IIn subclass showing strong intermediate-width emission features of H. The $\text{H}\alpha$ features had $\text{FWHM} \simeq 2000 \text{ km s}^{-1}$. We stress that this value does not directly reflect a characteristic fluid velocity value due to the ambiguity of the interpretation of the line widths which are affected by several broadening mechanisms (see Smith et al. 2010; CWV12). SN 2006tf exhibited spectroscopic similarities

with other SLSNe such as SN 2006gy (Smith et al. 2007) and SN 2008am (Chatzopoulos et al. 2011), and given the duration of its observed LC, it is considered a classic example of a Type IIn event associated with a massive progenitor (Smith et al. 2008). In this study we use the available KAIT *R*-band LC of SN 2006tf converted to bolometric luminosity ($BC = 0$).

3.2.3. SN 2008am

SN 2008am was another bright explosion discovered by the ROTSE Supernova Verification Project (RSVP; Chatzopoulos et al. 2011). The ROTSE-IIIb telescope followed up SN 2008am photometrically for over ~ 150 days. The spectra determine the redshift of the event to be $z = 0.2338$. For standard Λ -CDM cosmology this redshift translates to a distance of $\simeq 1121$ Mpc, making SN 2008am one of the most luminous explosions discovered with peak ROTSE magnitude -22.3 mag. The spectra show classic Type IIn Balmer and He I emission lines with typical FWHM ~ 1000 km s $^{-1}$. As for the case of SN 2006gy and SN 2006tf, the width of the emission lines may be attributable to electron scattering effects and not to true bulk kinematic motion. Chatzopoulos et al. (2011) used the ROTSE LC of SN 2008am to determine the explosion date of $MJD_{\text{expl}} = 54,438.8 \pm 1$.

For the purposes of this work, we analyze the ROTSE LC, which has many data points and contains data on the rise. This use of the ROTSE LC is in accord with the analysis we did for other events discussed here. We convert the ROTSE LC to a pseudo-bolometric one assuming $BC = 0$.

3.2.4. SN 2008es

Another bright SLSN discovered by ROTSE-IIIb and the RSVP program was SN 2008es (Gezari et al. 2009). The ROTSE-IIIb telescope managed to capture this event before maximum light, which allowed Gezari et al. (2009) to constrain the explosion date of the event ($MJD_{\text{expl}} = 54,574 \pm 1$). Post-maximum photometric observations of SN 2008es were obtained in IR (PAIRITEL; Miller et al. 2009), optical (KAIT, Nickel, PFC, UVOT; Miller et al. 2009 and P60, P200; Gezari et al. 2009), and UV (UVOT; Miller et al. 2009) bands, which allowed a comprehensive study of the event. SN 2008es was followed up spectroscopically for over ~ 100 days and exhibited a slow spectroscopic evolution with nearly featureless spectra in the first ~ 20 days after maximum with H α emission appearing only in the nebular spectra. This, together with the approximately linear decline of the optical LC (in magnitude scale), led Miller et al. (2009) to classify SN 2008es as a Type IIL explosion. The spectra revealed the redshift of the SN to be $z = 0.213$ (Miller et al. 2009) with characteristic velocities of $\sim 10,000$ km s $^{-1}$, which is the value we use for reference here. P Cygni features were detected in the nebular spectra for the H and He emission lines and became more prominent as the event evolved, indicating photospheric expansion. Although SN 2008es did not show classic SN IIn features, CSM interaction was considered as the most likely candidate for the event by Miller et al. (2009) and Gezari et al. (2009). They argue that an initially dense CSM can account for the absence of characteristic CSM interaction emission features. Kasen & Bildsten (2010) considered a magnetar model as an explanation for SN 2008es, which, although it provides a good fit to the LC, may have difficulty in accounting for the spectroscopic features (but see Dessart et al. 2012 for a different conclusion). We use the P60 *r* band together with the ROTSE unfiltered observations to assemble the pseudo-bolometric LC of SN 2008es.

3.2.5. CSS100217:102913+404220

CSS100217:102913+404220 (hereafter CSS100217) was discovered on 2010 February 17 (Drake et al. 2011). Drake et al. (2011) determine the redshift of the host of CSS100217 spectroscopically to be 0.147, implying a distance of 680.4 Mpc for the event assuming standard Λ -CDM cosmology. At this distance, and assuming Milky Way extinction of $E(B - V) = 0.1426$ at the position of the SN, the absolute magnitude of CSS100217 is $M_V = -22.7$ approximately 45 days after the discovery, corresponding to an optical luminosity of 1.3×10^{45} erg s $^{-1}$, making the event one of the most luminous ever discovered. Multi-wavelength photometry was obtained through the course of the transient in the radio, near-IR, optical, and UV. The transient was also detected by the *Swift* XRT in the 0.2–10 keV band as a soft source. The photometric data yield a total radiated energy of $\sim 1.2 \times 10^{52}$ erg over a period of ~ 287 rest-frame days. The spectra of CSS100217 are similar to those of SN 2008iy and other Type IIn SNe and show narrow Balmer emission lines indicating that the mechanism that powered that event is most likely strong interaction of SN ejecta with a massive CSM medium. Drake et al. (2011) also consider alternative scenarios such as active galactic nucleus variability or a tidal disruption event, which they rule out based on arguments related to the spectroscopic evolution of the event.

We convert the CSS LC of CSS100217 (which corresponds to *V* magnitudes) to bolometric in accord with Equation (1) of Drake et al. (2011) and the assumptions discussed therein. The conversion yields a peak luminosity of $\sim 4 \times 10^{44}$ erg s $^{-1}$, consistent with the one cited by Drake et al. (2011), at ~ 73 days after explosion in the rest frame assuming $MJD_{\text{expl}} = 55,160$, the time that the first real detection of the transient was recorded.

3.3. Hydrogen-deficient Superluminous Events (SLSN-I)

3.3.1. SN 2005ap

SN 2005ap was the first SLSN discovered by the Robotic Optical Transient Search Experiment (ROTSE) telescopes of the TSS program (Quimby et al. 2007). The only available LC of SN 2005ap was that taken from the ROTSE-IIIb telescope. Even though the signal-to-noise ratio was moderate, the post-maximum evolution of the LC of SN 2005ap shows a fast decline. The exact explosion date of the event is not well constrained, but Quimby et al. (2007) adopt a value 7–21 days before maximum based on comparisons with SN IIL template LCs. Spectra of SN 2005ap showed broad P Cygni features of C, N, and O that correspond to a velocity of $\sim 20,000$ km s $^{-1}$. The spectra also indicate a redshift of $z = 0.2832$ for SN 2005ap, which means that the peak absolute unfiltered magnitude of SN 2005ap was -22.6 mag. Quimby et al. (2011) put SN 2005ap in the same category as the recently discovered peculiar transients SCP06F6 (Barbary et al. 2009), PTF09cwl, PTF09cnd, and PTF09atu. Recently, Ginzburg & Balberg (2012) presented an SN ejecta–CSM interaction scenario for SN 2005ap in which the LC of the event is the result of the violent collision between equal mass ($\sim 15 M_{\odot}$) SN ejecta and steady-state wind (r^{-2}) CSM. Here we consider an $s = 0$ constant density CSM shell instead that may be more consistent with episodic, LBV-type mass loss that is implied by the high mass-loss rate suggested for the event. Again, we convert the SN 2005ap ROTSE LC to rest-frame pseudo-bolometric LC by assuming zero bolometric correction ($BC = 0$).

Table 3
Best-fit Parameters for the RD Model

SN	t_{rise} (days)	M_{Ni} (M_{\odot})	t_d (days)	χ^2/dof^a	M_{ej}^b (M_{\odot})
SN2008iy	315.00 (2.38)	13.18 (0.13)	509.30 (4.49)	0.44	363.60
PTF09uj	5.00 (0.06)	0.234 (0.002)	3.00 (0.02)	5.63	0.01
SN2006gy	56.00 (0.08)	22.76 (0.24)	56.81 (0.43)	13.76	4.50
SN2006tf	53.88 (0.50)	5.94 (0.03)	46.47 (0.52)	1.94	3.00
SN2008am	44.00 (7.85)	20.45 (13.82)	39.11 (32.53)	1.51	2.14
SN2008es	22.00 (2.36)	16.07 (0.60)	19.79 (1.98)	4.96	0.55
CSS100217	115.40 (5.60)	104.60 (4.70)	127.50 (7.81)	6.53	22.78
SN2005ap	16.00 (0.40)	15.98 (0.33)	13.68 (0.42)	0.60	0.26
SCP06F6	24.00 (4.55)	17.15 (1.19)	28.09 (4.91)	8.30	1.10
SN2007bi	27.00 (14.22)	9.46 (1.32)	25.19 (14.29)	2.40	0.90
SN2010gx	21.18 (0.24)	12.97 (0.50)	31.12 (0.50)	3.47	5.17
SN2010kd	59.00 (3.15)	12.35 (1.13)	60.76 (5.52)	0.17	8.50

Notes. The numbers in parentheses indicate the corresponding 1σ uncertainties of the fitting parameters. Parameters without cited errors indicate derived physical parameters.

^a χ^2 per degree of freedom ($\text{dof} = N_d - N_p - 1$, where N_d is the number of data points and N_p is the number of fitting parameters).

^b Using Equation (3) and assuming $v = 10,000 \text{ km s}^{-1}$, $\kappa = 0.33 \text{ cm}^2 \text{ g}^{-1}$.

3.3.2. SCP06F6

SCP06F6 was a controversial transient discovered by Barbary et al. (2009). The LC of SCP06F6 was constructed by observations in the F850LP (similar to SDSS z') and F775W (similar to SDSS i') filters of the Advanced Camera for Surveys Wide-Field Camera mounted on the *Hubble Space Telescope*. The LC of SCP06F6 is fairly symmetric in shape with a rise timescale close to its decline timescale. The redshift of SCP06F6 remained unknown for over two years due to its peculiar spectrum. Three optical spectra obtained with the Very Large Telescope Low Dispersion Spectrograph 2, Keck-LRIS, and Subaru-FOCAS showed unidentified broad absorption features in the blue. Works by Gänsicke et al. (2009), Soker et al. (2010), and Chatzopoulos et al. (2009) made attempts to identify the nature of these features and determine the redshift of SCP06F6, unsuccessfully. Quimby et al. (2011) associated the spectrum of SCP06F6 with spectra of other similar recently discovered PTF transients (PTF09cwl, PTF09cnd, and PTF09atu) and determined the redshift of SCP06F6 to be $z = 1.189$. The same work identified the controversial broad spectral features as Fe/Co blends and Ni III, O II, and Si III lines.

Using the observed broadband LCs of SCP06F6, we construct the rest-frame pseudo-bolometric LC following the technique described in Chatzopoulos et al. (2009) for the currently accepted redshift of the event ($z = 1.189$; Quimby et al. 2011).

3.3.3. SN 2007bi

Gal-Yam et al. (2009) reported the discovery of the best candidate for a PISN explosion to date, SN 2007bi, by the Supernova Factory program (Aldering et al. 2009). Palomar-60 (P60) R -band photometry of SN 2007bi was obtained for over a ~ 130 day period at the rest frame of the SN. The explosion date of SN 2007bi is uncertain, which induces an uncertainty in the models applied to explain the LC of the event. We adopt as a reference value $\text{MJD}_{\text{expl}} = 54,089$, which is 70 days before peak R magnitude, in accordance with the range proposed by Gal-Yam et al. (2009). The explosion date will be a fitting parameter for the LC of this SN in our work. The spectra of SN 2007bi do not show signs of CSM interaction, and H and He

features are not detected. Strong Ca, Mg, and Fe features and Ni/Co/Fe blends are identified close to the near-UV part of the spectrum (Gal-Yam et al. 2009). Spectral fits provide us with an estimate of the characteristic velocity of $v = 12,000 \text{ km s}^{-1}$. The lack of H and He features led to the classification of this event as an SN Ic explosion. Also, the lack of evidence for an SN II in CSM interaction and the long duration and high luminosity of the event make it a good candidate for a PISN explosion (Gal-Yam et al. 2009). Other proposed models for SN 2007bi are an energetic core-collapse explosion (Moriya et al. 2010) and a magnetar spin-down model developed by Kasen & Bildsten (2010) and Woosley (2010). Recently, the possibility of H-poor CSM interaction as a model for SLSN-I events, including SN 2007bi, has also been suggested (Chatzopoulos & Wheeler 2012). We constructed the pseudo-bolometric LC of SN 2007bi using the available P60 R -band LC of SN 2007bi presented in Table 3 of Gal-Yam et al. (2009), a Milky Way extinction of $A_R = 0.07$ mag from the NED database at the location of the transient, and the observed redshift $z = 0.1279$. All these values yield an absolute peak luminosity of $1.11 \times 10^{44} \text{ erg s}^{-1}$ for SN 2007bi.

3.3.4. SN 2010gx

SN 2010gx was discovered on 2010 March 13 at 18.5 mag by the CRTS team (Mahabal et al. 2010; Pastorello et al. 2010). Independent discovery was later announced by the PTF survey (Quimby et al. 2010). The host of SN 2010gx is identified as a faint galaxy in the SDSS images, and its redshift is estimated to be 0.23. For standard Λ -CDM cosmology this redshift translates to a distance of $\simeq 1120$ Mpc, making this object yet another member of the class of SLSNe ($M_{B,\text{peak}} \simeq -21.2$). Extensive photometric follow-up was obtained in the $ugriz$ bands using a variety of telescopes (Pastorello et al. 2010), which provided an estimate for the explosion date of the event to be $\text{MJD}_{\text{expl}} = 55,260$, yielding a rise time to maximum light of ~ 16 days in the rest frame.

The pre-maximum spectra of SN 2010gx show a blue continuum ($T_{\text{BB}} = 15,000 \pm 1700 \text{ K}$) with broad absorption features in the bluer parts. Later spectra also show broad P Cygni absorptions of Ca II, Fe II, and Si II, which led to classification of

the object as an SN Ib/c. Pastorello et al. (2010) have difficulty suggesting a model that accounts for the overall characteristics of SN 2010gx (spectral evolution, fast evolution of LC, peak luminosity) and suggest that most scenarios (^{56}Ni decay powered core-collapse SN, PISN, PPISN, or magnetar-powered SN) do not comfortably match the event. Therefore, here we attempt to re-visit those models in more detail and also consider CSM interaction as an alternative. SN ejecta interaction with a dense r^{-2} wind as the power mechanism for SN 2010gx was recently considered by Ginzburg & Balberg (2012), who presented hydrodynamics simulations of such phenomena that take into account the effects of radiation diffusion and calculate model LCs. Ginzburg & Balberg determined that collision of $\sim 15 M_{\odot}$ of SN ejecta (with energy $E_{\text{SN}} = 2 \times 10^{51}$ erg) with $\sim 15 M_{\odot}$ of a steady-state CSM wind that terminates at a radius of 2.5×10^{15} cm reproduced well the observed LC and blackbody temperature evolution of SN 2010gx. The implied average mass-loss rate for their parameters assuming a fiducial wind velocity of 10 km s^{-1} is $\dot{M} = 0.2 M_{\odot} \text{ yr}^{-1}$, which is inconsistent with steady-state, quiescent mass loss and more in accord with episodic, LBV-type mass loss that, in turn, does not necessarily lead to an r^{-2} density profile for the CSM. Here we will consider CSM interaction with an $s = 0$ constant density CSM shell that might be more consistent with non-steady mass-loss.

We converted the r -band LC of SN 2010gx to pseudo-bolometric assuming $\text{BC} = 0$, $E(B - V) = 0.04$ (Schlegel et al. 1998), and $E(B - V)_{\text{host}} = 0$ (Pastorello et al. 2010).

3.3.5. SN 2010kd

The ROTSE-IIIb telescope of the RSVP project discovered SN 2010kd on 2010 November 14 (Vinko et al. 2010) at a magnitude of ~ 17 mag. Spectra obtained by the Hobby-Eberly Telescope and Keck showed narrow $\text{H}\alpha$ emission, which helped constrain the redshift of the object at $z = 0.101$, implying an absolute ROTSE magnitude of ~ -21 , suggesting the event is superluminous. The transient was followed up photometrically in the $UBVRI$ filters and in the UV and X-ray by *Swift* UVOT and the XRT. The SN was detected as a strong UV source, but no X-ray flux was measured. The photometric observations and the date of discovery provide an estimate for the actual explosion date at $\text{MJD}_{\text{expl}} = 55,483$, implying a rest-frame rise time to peak luminosity of ~ 60 days (Vinko et al. 2010; J. Vinko et al., in preparation). The observed spectroscopic evolution of SN 2010kd implies a behavior similar to SN 2007bi with a lack of H and He features and presence of C II, O I, O II, and possibly Co III making it an SLSN-I event, and a PISN candidate. We converted the V -band LC of SN 2010kd to pseudo-bolometric assuming $\text{BC} = 0$, $E(B - V) = 0.0213$ (Schlegel et al. 1998), which implies a peak luminosity of $\sim 10^{44}$ erg s^{-1} .

4. FITS TO OBSERVED LIGHT CURVES OF SLSNe

In this section we attempt to fit the semi-analytical LC models that are given by Equations (1), (2), (4), and (7) to the observed LCs of some interesting SN events, in order to understand which mechanism best describes their nature.

4.1. The Fitting Method

The semi-analytic LC models described in Section 2 were fitted to the observed data by applying a χ^2 -minimization code MINIM that was developed by two of us (Z.L.H. and J.V.) and implemented in C++. MINIM uses a controlled random-search technique, the Price algorithm (Brachetti et al. 1997), which has

been extensively tested and applied for solving global optimization problems. The algorithm treats the unknown parameters as random variables in the N_p -dimensional hyperspace, where N_p is the number of parameters. The boundaries of the permitted values for each parameter are defined as $p_i(\text{low})$ and $p_i(\text{high})$ and given to the code in the input file. The aim of the algorithm is to find the global minimum of the χ^2 function within this permitted parameter volume.

After reading the input data, the code randomly selects N_r vectors in the parameter hyperspace. Each vector is defined as $\mathbf{p} = (p_1, p_2, \dots, p_{N_p})$, and each p_i parameter is chosen as an equally distributed random number between $p_i(\text{low})$ and $p_i(\text{high})$. For each \mathbf{p} vector the value of χ^2 is calculated. We have applied $N_r = 200$, which was found to be a good compromise between reliable convergence (i.e., finding the global minimum χ^2) and computation speed. The algorithm then chooses a new trial \mathbf{p} vector by combining a randomly chosen subset of $N_p + 1$ elements from the stored vectors, and compares their χ^2 value with those of the stored vectors. If a vector with a better χ^2 is found, then the one with the highest χ^2 in the stored vector set is replaced by this new vector. This process is iterated until the difference between the χ^2 values of the stored vectors is less than $\Delta\chi^2 = 1$.

As a final step, the Levenberg–Marquardt algorithm is applied to fine-tune the parameters in the lowest χ^2 vector produced by the Price algorithm. The result of this routine is accepted as the best-fitting model parameter set. The uncertainties of the fitted parameters are estimated by calculating the standard deviation of each p_i parameter in the final set of the N_r random vectors around the best-fitting vector. Our tests with simple analytic functions and simulated data have shown that this kind of error estimate is consistent with using the full covariance matrix of the χ^2 hypersurface. An extensive discussion of parameter correlation and degeneracy as calculated by MINIM in the case of the CSM+RD model is presented in the Appendix.

We note that in some cases the fitting is ill-constrained due to the small number of data points and the presence of many fitting parameters, resulting in a low value of the degree-of-freedom $N_{\text{data}} - N_p$. Estimates for the diffusion or SN ejecta mass, M_{ej} , provided by Equation (3) for the RD, MAG, and TH models, are uncertain because of the uncertainty in the optical opacity, κ , but also due to the intrinsic uncertainty in the fitted value for the LC timescale, t_d , which is dependent upon the explosion time, t_{ini} (which is also ill-constrained for SLSNe).

For the hybrid CSM+RD model we assume and fix $\delta = 2$ and $n = 12$ for the SN ejecta inner and outer power-law density profile slopes, respectively, in all cases. The range in fitted parameters for various models that gives approximately equally good fits yields some notion of the range of parameters in viable model space. Ideally, we would incorporate the density slope of the CSM, s , as a parameter to be fitted. This can be done, but substantially increases the computation time. Here we have investigated two relevant values of s , 0 and 2, and randomly varied other parameters.

A summary of the fitting parameters is given in Tables 3–7, and the fits are presented in Figures 2, 3, and 4. Tables 3, 4, and 5 present the RD, MAG, and TH model fitting parameters for all events. The normal IIn, SLSN-II, and SLSN-I events in each table are separated by straight lines. Tables 6 and 7 present the CSM+RD model fitting parameters for H-rich and H-poor events, respectively. For each class of models we characterize and discuss issues of parameter correlation and hence degeneracy that make it difficult to determine unique

Table 4
Best-fit Parameters for the MAG Model

SN	t_{rise} (days)	E_p (10^{51} erg)	t_p (days)	t_d (days)	R_0 (10^{13} cm)	χ^2/dof	M_{ej}^b (M_{\odot})	P_i (ms)	B (10^{14} G)
SN2008iy	292.00 (2.28)	1.39 (0.05)	101.90 (10.48)	342.20 (6.74)	31.20 (15.81)	0.40	164.13	3.79	0.62
PTF09uj	5.00 (0.08)	0.02 (0.01)	5.00 (0.16)	4.36 (0.12)	0.01 (0.37)	0.05	0.03	29.17	28.42
SN2006gy	49.06 (0.21)	4.10 (0.10)	12.67 (0.06)	65.49 (0.02)	2.00 (0.80)	12.78	6.01	2.21	1.35
SN2006tf	65.00 (1.09)	1.09 (0.01)	58.91 (1.40)	58.92 (0.60)	2.49 (1.68)	2.83	4.87	4.28	1.22
SN2008am	41.03 (0.03)	4.07 (0.02)	134.40 (1.01)	26.88 (0.05)	0.11 (0.22)	1.58	1.01	2.22	0.42
SN2008es	20.00 (0.002)	2.43 (0.01)	47.31 (0.36)	14.21 (0.09)	0.04 (0.22)	2.87	0.28	2.87	0.91
CSS100217	112.00 (2.50)	17.18 (6.44)	216.10 (23.70)	82.24 (7.59)	85.26 (8.98)	0.78	9.45	1.08	0.16
SN2005ap	16.00 (0.69)	2.12 (0.07)	28.87 (4.29)	12.12 (1.20)	2.46 (0.91)	0.58	0.21	3.10	1.25
SCP06F6	28.70 (0.59)	3.21 (0.18)	9.59 (1.23)	38.63 (1.34)	32.46 (14.77)	3.09	2.09	2.50	1.76
SN2007bi	61.00 (0.87)	2.79 (0.04)	19.46 (0.60)	72.51 (0.70)	2.36 (0.90)	2.25	7.37	2.67	1.32
SN2010gx	14.00 (0.20)	1.49 (0.03)	1.01 (0.01)	35.22 (0.18)	9.97 (0.28)	0.30	1.74	3.66	7.98
SN2010kd	47.99 (1.63)	2.66 (0.10)	8.06 (1.80)	70.20 (3.50)	2.55 (1.10)	0.13	6.91	2.74	2.10

Note. See comments for Table 3.

Table 5
Best-fit Parameters for the TH Model

SN	t_{rise} (days)	E_{sh} (10^{51} erg)	t_{sh} (days)	t_d (days)	χ^2/dof	$M_{\text{CSM,th}}^b$ (M_{\odot})
SN2008iy	31.00 (1.63)	0.74 (0.02)	30.48 (26.55)	461.70 (8.89)	1.92	298.77
PTF09uj	5.00 (0.11)	0.01 (0.01)	4.68 (0.21)	8.37 (0.24)	0.25	0.09
SN2006gy	60.00 (0.08)	1.34 (0.01)	60.55 (0.51)	51.36 (0.25)	13.72	3.70
SN2006tf	14.00 (5.23)	0.74 (0.07)	13.80 (11.57)	95.13 (0.52)	3.80	12.68
SN2008am	37.00 (1.63)	2.37 (0.02)	36.80 (2.14)	103.70 (1.29)	1.52	15.07
SN2008es	34.00 (11.13)	1.57 (0.10)	34.16 (15.29)	42.29 (1.86)	1.28	2.51
CSS100217	118.20 (0.65)	11.92 (0.08)	83.58 (0.94)	248.20 (2.50)	1.55	86.34
SN2005ap	12.12 (4.68)	1.32 (0.09)	21.5 (5.16)	29.10 (1.35)	0.54	1.17
SCP06F6	43.01 (0.45)	1.15 (0.02)	45.50 (0.75)	27.94 (1.25)	1.65	2.90
SN2007bi	2.00 (28.20)	0.99 (0.06)	48.80 (7.30)	70.15 (0.59)	2.60	6.90
SN2010gx	47.00 (0.34)	0.45 (0.01)	46.93 (0.39)	20.32 (0.18)	1.36	0.58
SN2010kd	69.00 (5.55)	0.73 (0.02)	69.27 (6.89)	52.39 (0.74)	0.27	3.85

Note. See comment for Table 3.

parameter fits. Correlation usually increases the parameter uncertainty. We took this into account in our calculations, and the errors reported in the tables reflect the parameter correlations.

4.2. Radioactive Diffusion (RD) Models

The RD model fitting and derived parameters for all events in our sample are listed in Table 3. As can be seen, but also speculated before (Smith et al. 2007; Chatzopoulos et al. 2012; Gal-Yam 2012), almost no SLSN event can be powered solely by the radioactive decays of ^{56}Ni and ^{56}Co due to the unphysical result of $M_{\text{ej}} < M_{\text{Ni}}$. We stress, however, that the estimation of M_{ej} using Equation (3) is uncertain given that our cited M_{ej} values all assume $v = 10,000$ km s $^{-1}$ and $\kappa = 0.33$ cm 2 g $^{-1}$. For the SLSN-II events this choice for the optical opacity of the SN ejecta is reasonable (but note that prior to ionization the opacity of the CSM is likely to be much less). For SLSN-I events a lower opacity value of $\kappa \simeq 0.1$ cm 2 g $^{-1}$ (Valenti et al. 2008) may be more appropriate. Such a choice would increase the M_{ej} estimates for SLSN-I by a factor of 3. Even in that case, the $M_{\text{ej}} < M_{\text{Ni}}$ inconsistency would still hold for most SLSN-I events. SN 2010gx and SN 2010kd may be exceptions, but even their results would imply that most of the SN ejecta are made of ^{56}Ni , still an extraordinary condition. Some authors (Gal-Yam et al. 2009) have adopted an even lower opacity value

($\kappa = 0.05$ cm 2 g $^{-1}$) that leads to even higher SN ejecta mass estimates (by a factor of 6.6) than the values shown in Table 1. The Thompson scattering opacity in an ejecta that lacks both H and He is uncertain and will depend not only on the chemical composition, but also on ionization conditions. It is difficult to constrain this parameter without a detailed model of the ejecta, which is beyond the scope of this paper. In addition to the ejecta and nickel mass constraints, it can be seen in Figures 2–4 that for many events the very late time-decline rate is not well reproduced by RD models.

The fitted value of the LC timescale, t_d , also has a major impact on the estimated M_{ej} . As noted before, for many of the events in our sample (specifically SN 2006tf, SN 2007bi, SN 2008iy, SN 2010kd) we lack LC data during the phase of the rise to peak luminosity, and we therefore lack an accurate estimate of the explosion dates of the events. For this reason, in our fitting procedure we let the explosion date (and, as a result, the rise time to maximum light, t_{rise}) be a fitting parameter as well, but constrained within a range of values suggested by the discoverers of each particular event based on pre-explosion upper limits. Note that since the explosion date (t_0) is a parameter that is not related to the physics of a particular SN, in Table 3 we present the rise time ($t_{\text{rise}} = t_{\text{max}} - t_0$) instead. The fitted explosion dates therefore have a direct effect on the fitted t_d values. As we show in detail in the Appendix (Table 9), in our

Table 6
Summary of the Fitting Parameters for the CSM+RD SN LC Model to the Hydrogen-rich Events

Parameter	SN 2008iy	PTF 09uj ($s = 0$)	PTF 09uj ($s = 2$)	SN 2006gy ($s = 0$)	SN 2006gy ($s = 2$)	SN 2006tf	SN 2008am	SM 2008es	CSS100217
t_{rise} (days)	241.00 (4.64)	6.00 (0.19)	5.00 (0.10)	67.12 (0.09)	29.00 (0.04)	45.00(1.19)	28.99 (1.30)	21.00 (0.21)	71.34 (0.86)
v_{SN} (10^3 km s^{-1})	5.99 (0.81)	21.46 (0.27)	13.33 (0.17)	35.24 (0.11)	31.57 (0.47)	27.08 (0.82)	45.29 (0.98)	61.85 (0.62)	35.46 (0.10)
M_{ej} (M_{\odot})	36.31 (8.65)	1.52 (0.08)	37.39 (2.33)	10.70 (0.08)	7.87 (31.17)	33.58 (1.65)	47.77 (7.58)	11.90 (0.33)	100.2 (0.4)
R_p (10^{13} cm)	42.89 (5.65)	8.67 (0.55)	32.59 (1.67)	53.12 (3.83)	1.57 (0.10)	36.62 (2.92)	36.56 (3.57)	45.28 (3.40)	99.94 (0.85)
M_{CSM} (M_{\odot})	38.58 (1.66)	0.03 (0.01)	0.16 (0.01)	5.18 (0.15)	3.64 (0.07)	4.72 (0.33)	4.90 (0.30)	2.69 (0.12)	78.27 (0.65)
$\rho_{\text{CSM},1}$ ($10^{-12} \text{ g cm}^{-3}$)	0.29 (0.14)	99.37 (23.93)	1.57 (0.29)	0.04 (0.01)	573.00 (282.00)	3.15 (0.80)	3.70 (1.55)	0.86 (0.23)	0.15 (0.01)
M_{Ni} (M_{\odot})	2.44 (0.26)	0.28 (0.04)	0.32 (0.10)	3.25 (0.04)	3.80 (0.50)	0.00 (0.04)	1.57 (1.30)	0.04 (0.06)	0.50 (0.43)
χ^2/dof	0.35	0.05	0.05	4.87	49.30	3.80	1.52	1.27	1.15
E_{SN} (10^{51} erg)	0.17	0.09	0.85	1.70	1.00	3.15	12.54	5.82	83.58
$M_{\text{CSM,th}}$ (M_{\odot})	38.37	0.03	0.15	4.97	3.45	4.71	4.89	2.67	77.42
R_{ph} (10^{14} cm)	40.06	0.93	4.74	40.51	37.55	9.14	8.74	12.21	63.44
R_{CSM} (10^{14} cm)	40.13	0.93	4.76	41.07	39.60	9.15	8.74	12.24	63.67
τ_{CSM}	337	272	53	44	2960	571	620	218	266
$t_{\text{RS},*}$ (days)	458.61	6.34	505.86	104.68	51.23	44.83	28.37	22.53	73.13
$t_{\text{FS,BO}}$ (days)	438.47	0.07	4.84	66.98	86.91	10.56	5.61	6.94	56.36

Note. For the CSM+RD best-fit models we have adopted $\delta = 2$ and $n = 12$.

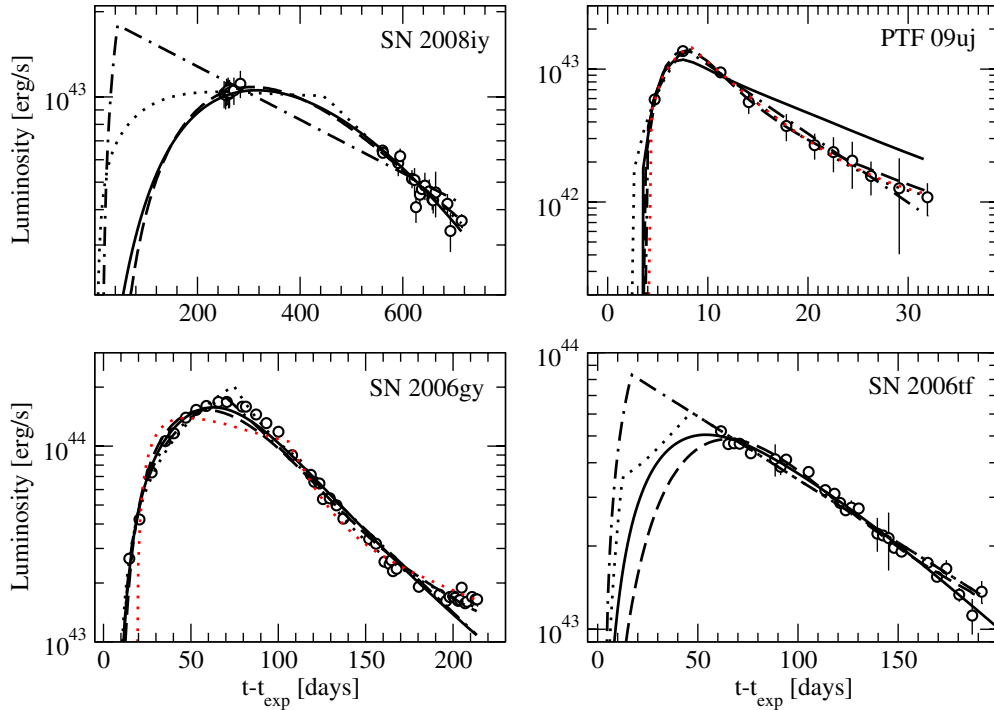


Figure 2. Lowest χ^2 model fits to the observed LCs of SN 2008iy (upper left panel), PTF 09uj (upper right panel), SN 2006gy (lower left panel), and SN 2006tf (lower right panel). Solid curves correspond to the RD model, dashed curves to the MAG model, dashed-dotted curves to the TH model, and dotted curves to the hybrid CSM+RD model in the case of constant density CSM shell ($s = 0$). The red dotted curves show the best-fit CSM+RD model for the choice $s = 2$ (steady-state wind CSM); this model is inferior to all the others for SN 2006gy. Parameters of the best-fit models are given in Tables 3–7.

(A color version of this figure is available in the online journal.)

Table 7
Summary of the Fitting Parameters for the CSM+RD SN LC Model to the Hydrogen-poor Events

Parameter	SN 2005ap	SCP 06F6	SN 2007bi	SN 2010gx ($s = 0$)	SN 2010gx ($s = 2$)	SN 2010kd
t_{rise} (days)	15.00 (0.94)	39.39 (0.94)	59.00 (1.25)	43.00 (0.37)	31.00 (0.16)	58.00 (1.10)
v_{SN} (10^3 km s^{-1})	72.24 (1.60)	43.46 (0.64)	29.96 (0.90)	37.24 (0.68)	30.37 (0.11)	30.01 (0.57)
M_{ej} (M_{\odot})	7.36 (0.72)	7.55 (0.39)	44.27 (2.61)	17.59 (0.78)	9.70 (0.26)	34.10 (1.91)
R_p (10^{13} cm)	27.48 (3.84)	34.98 (7.92)	31.28 (4.98)	93.50 (5.07)	2.00 (1.51)	43.25 (5.31)
M_{CSM} (M_{\odot})	1.19 (0.07)	4.08 (0.22)	4.28 (0.26)	1.39 (0.05)	1.64 (0.26)	3.28 (0.15)
$\rho_{\text{CSM},1}$ ($10^{-12} \text{ g cm}^{-3}$)	1.07(0.68)	0.05(0.03)	1.34(1.21)	0.03 (0.01)	1664.30 (975.90)	1.09 (0.66)
M_{Ni} (M_{\odot})	3.56 (1.48)	0.00 (0.28)	0.57 (0.22)	0.00 (0.01)	0.00 (0.01)	0.00 (0.15)
χ^2/dof	0.53	0.61	2.60	1.88	0.98	0.27
E_{SN} (10^{51} erg)	4.91	5.11	5.08	3.12	1.14	3.93
$M_{\text{CSM,th}}$ (M_{\odot})	1.18	3.84	4.26	1.37	1.61	3.26
R_{ph} (10^{14} cm)	8.18	33.35	11.55	12.00	15.50	11.47
R_{CSM} (10^{14} cm)	8.20	34.03	11.57	12.00	15.80	11.49
τ_{CSM}	117	30.5	227	2	6573	157
$t_{\text{RS,*}}$ (days)	14.53	49.10	59.00	42.88	57.93	57.90
$t_{\text{FS,BO}}$ (days)	4.12	34.03	14.97	2.64	33.37	12.07

Note. Same as Table 6.

fitting procedure we recover this strong correlation between t_d and t_{rise} . These parameters are often similar, but not identical.

A major impact of the explosion date uncertainty is observed in the case of the PISN candidate SN 2007bi. Using the Gal-Yam et al. (2009) adopted value of $t_d = 70$ days, with $v = 10,000 \text{ km s}^{-1}$ and $\kappa = 0.1 \text{ cm}^2 \text{ g}^{-1}$ appropriate for H-poor SN ejecta, we obtain $M_{\text{ej}} = 22.6 M_{\odot}$ while, for $\kappa = 0.05 \text{ cm}^2 \text{ g}^{-1}$, $M_{\text{ej}} = 45.3 M_{\odot}$. For the lower choice of opacity and this t_d value, we recover the results of Gal-Yam et al. (2009), Moriya et al. (2010), and Yoshida & Umeda (2011), which imply that models of PISN or energetic core-collapse supernova (CCSN) may be consistent with SN 2007bi in terms of the LC, since $M_{\text{ej}} \gg M_{\text{Ni}}$. Taking

into account the uncertainty in the explosion date, however, our fitting derived a much smaller value for t_d (25.2 days) for which no reasonable choice for κ satisfies the physical $M_{\text{ej}} > M_{\text{Ni}}$ solution. This result indicates that the nature of SN 2007bi and its interpretation as a PISN remain under debate. Given this uncertainty in the explosion date, PISN models for SN 2007bi that involve large amounts of ^{56}Ni are possible, at least in terms of the LC as noted by Gal-Yam et al. (2009). Scaling, the late, nebular spectrum of the archetypical broad-lined Type Ic SN 1998bw associated with a gamma-ray burst to match the nebular spectrum of SN 2007bi also suggests the production of substantial ^{56}Ni . Recent non-LTE radiation hydrodynamics

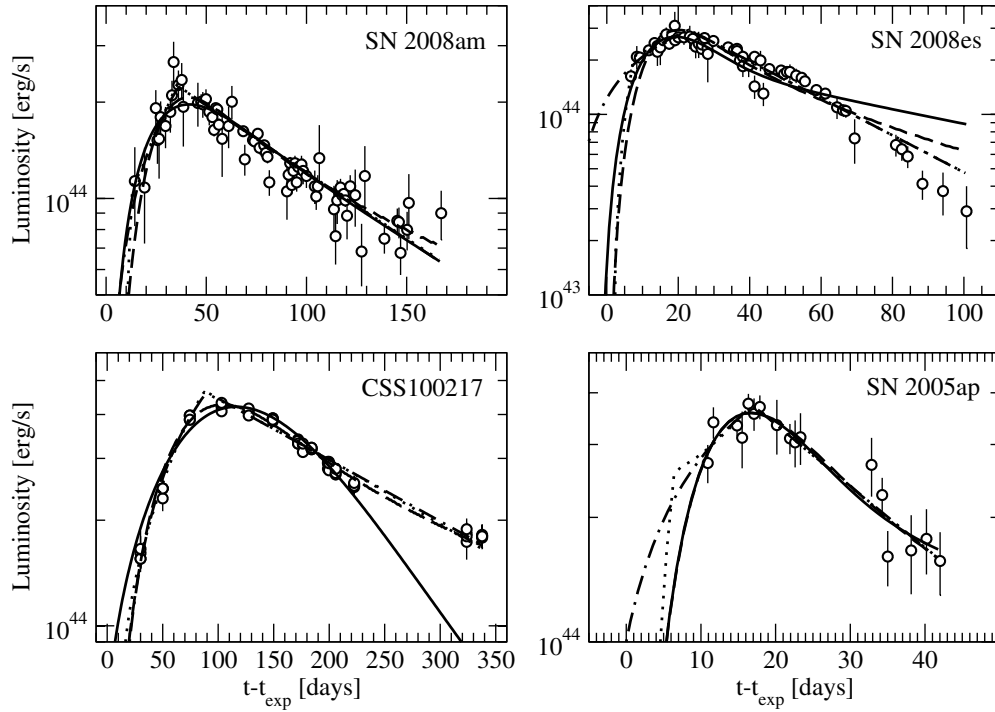


Figure 3. Same as Figure 2 but for SN 2008am (upper left panel), SN 2008es (upper right panel), CSS100217 (lower left panel), and SN 2005ap (lower right panel).

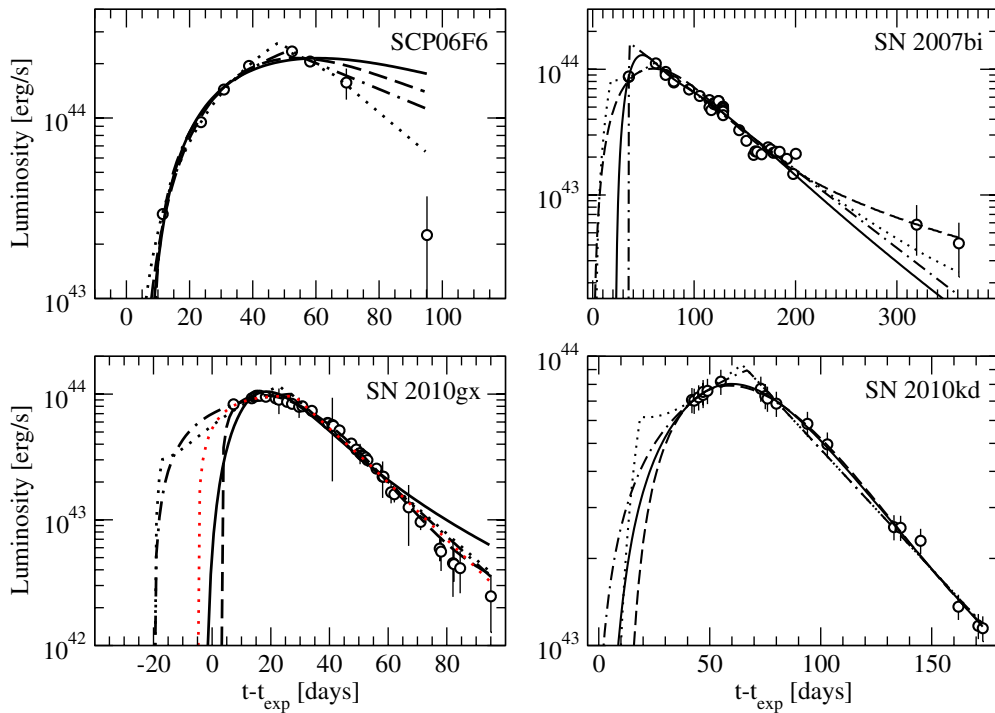


Figure 4. Same as Figure 2 but for SCP06F6 (upper left panel), SN 2007bi (upper right panel), SN 2010gx (lower left panel), and SN 2010kd (lower right panel). Negative $t - t_{\text{exp}}$ implies that the model has an earlier date for the explosion than the pre-selected fiducial t_{exp} value given in Table 2. (A color version of this figure is available in the online journal.)

models of PISNe (Dessart et al. 2013), however, show that the spectral evolution of SN 2007bi is inconsistent, in terms of color, temperature, and spectral features, with that expected for a PISN. We return to a discussion on alternative models for SN 2007bi in Sections 4.3 and 4.4.

Our fitting tests presented in detail in the Appendix indicate that the RD model fitting parameters are all correlated. In

Figure 5 (see also Table 9) the red points that represent models that fit the data in the parameter space are distributed along a line. If a fit fails to reproduce the exact (t_d, M_{Ni}) pair, the result may be a slightly different set of values for t_d and M_{Ni} that vary from the exact solution, but still fit the data reasonably well. The tightest correlations are observed between t_d and t_{rise} , as discussed above, but M_{Ni} and t_d are also correlated. The tight

Table 8
Summary of the Characteristics of the Sample of Transients Studied in This Work

Event	Type	Spectral Properties	Best-fit LC Model ^a
SN 2008iy	IIn	Pure H emission, weak P Cygni	CSM+RD/TH
PTF 09uj	IIn	Pure H emission weak P Cygni	CSM+RD/TH
SN 2006gy	IIn	P Cygni H	CSM+RD/TH
SN 2006tf	IIn	Pure H emission, weak P Cygni	CSM+RD/TH
SN 2008am	IIn	Pure H emission	CSM+RD/TH
SN 2008es	II-L?	P Cygni H	MAG, CSM+RD
CSS100217	IIn	Pure H emission, weak P Cygni	CSM+RD/TH
SN 2005ap	II-L	Broad P Cygni C, N, O	CSM+RD/TH
SCP06F6	?	Peculiar	CSM+RD/TH
SN 2007bi	Ic	Ni/Co/Fe blends, no H	RD, MAG, CSM+RD/TH
SN 2010gx	Ib/c	P Cygni CaII, FeII, SiII	CSM+RD/TH
SN 2010kd	Ic	Peculiar, no H, He	MAG, CSM+RD/TH

Note. ^a RD = ⁵⁶Ni and ⁵⁶Co radioactive decay diffusion model, MAG = Magnetar spin-down model, TH = “Top-hat” model and CSM+RD = Hybrid SN ejecta–CSM interaction plus ⁵⁶Ni and ⁵⁶Co decay model, CSM = SN ejecta–CSM interaction model (zero input from radioactive decays).

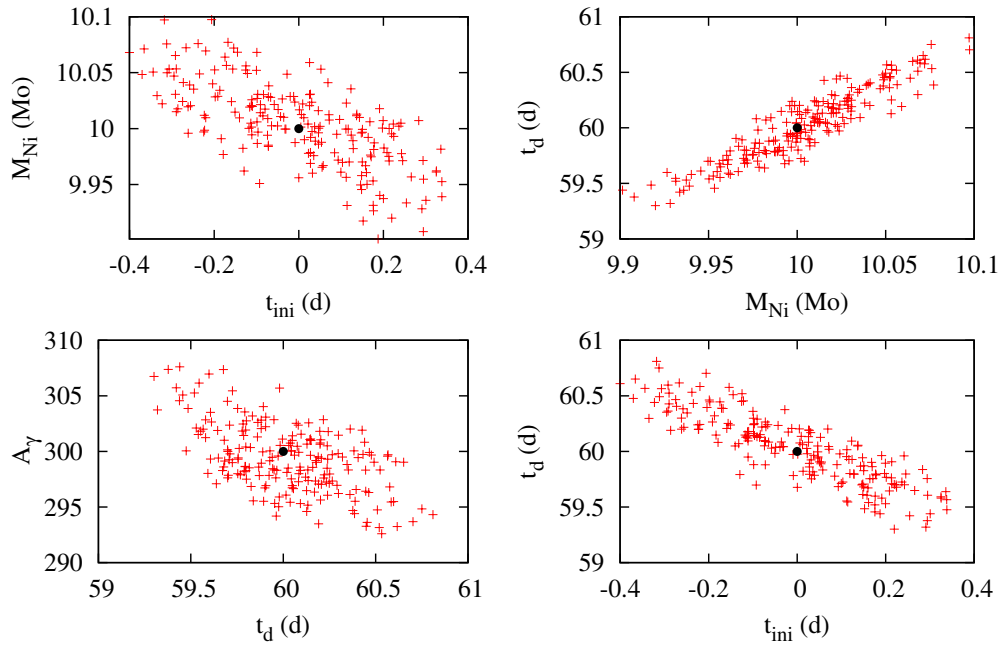


Figure 5. Distribution of random choices of parameters around the χ^2 minimum found by MINIM with respect to a generic specified RD model. The extension of the distribution is $\Delta\chi^2 = 1$ corresponding to the 67% confidence interval around the minimum (see Section 3). More elongated ellipsoids indicate stronger correlation between the parameters. A filled circle shows the position of the initial model. For the definition of the fitting parameters plotted here please see Appendix A.1. (A color version of this figure is available in the online journal.)

correlation between M_{Ni} and t_d reflects “Arnett’s rule” (A80 and A82), which is built into the RD model by design and implies that at LC peak the input and output powers are equal. For all RD models discussed here, the gamma-ray leakage parameter, A_γ , is so large and unconstrained that it is irrelevant and does not strongly affect the fitting results.

4.3. Magnetar (MAG) Models

Table 4 lists the final fitting and derived parameters for the MAG model for all events in our sample. The MAG model provides good, low reduced- χ^2 fits for the majority of SN LCs that we examine in this work. For all events, the B-field values

and initial magnetar periods implied are in ranges expected for magnetars ($B = (0.1\text{--}10) \times 10^{14}$ G, $P_i = 1\text{--}4$ ms) with the exception of PTF 09uj.

The MINIM fitting results for the MAG model also seem to be in reasonable agreement with the results of Kasen & Bildsten (2010) for the LCs of SN 2007bi and SN 2008es. For SN 2008es we derive a somewhat weaker B-field and a bit slower initial magnetar period. Our derived M_{ej} using fiducial values for ν and κ is much smaller than the $5 M_\odot$ presented by Kasen & Bildsten (2010). The discrepancy in the derived M_{ej} can be attributed to reasons similar to those discussed for the RD model (uncertain opacity and explosion time). For SN 2007bi our agreement with Kasen & Bildsten (2010) is much better (their fit gives

$B = 2.5 \times 10^{14}$ G, $P_i = 2$ ms, and $M_{ej} = 20 M_{\odot}$; our derived M_{ej} would become $24.3 M_{\odot}$ for the H-poor appropriate choice of $\kappa = 0.2 \text{ cm}^2 \text{ g}^{-1}$.

In the [Appendix](#) we discuss the parameter correlations for the MAG model. The MAG model version of the ‘‘Arnett rule’’ is also recovered here via strong correlations between the E_p , t_p , and t_d parameters. The strong anti-correlation between t_p and t_d is also suggested by Kasen & Bildsten (2010) and their Equation (16). As can be seen in Table 10, despite the strong correlations among most parameters of the MAG model, all parameters are well recovered in a test fitting done by MINIM.

The MAG model is not favored for SLSN-II events for which clear signs of CSM interaction are detected in the spectra in the form of intermediate and narrow-width emission lines. For SLSN-I events, the MAG model cannot be ruled out, at least in terms of quality of fit to the LCs. Non-LTE radiation hydrodynamics models recently presented by Dessart et al. (2012) suggest that the MAG model may indeed be relevant for events such as SN 2007bi, PTF 09atu (Quimby et al. 2011), and other SLSN-I under the basic assumption that the radiation from the magnetar thermalizes efficiently in the expanding SN ejecta (but see Bucciantini et al. 2006).

4.4. CSM Interaction (TH and CSM+RD) Models

The most successful models for SLSN LCs in terms of reduced- χ^2 values and physical consistency of the derived parameters are those for which the main power source is shock heating due to SN ejecta–CSM interaction. In our analysis here we assume that members of both SLSN-I and SLSN-II may be powered by CSM interaction. In the case of SLSN-II there are clear signs of such interaction in the optical spectra of these objects, specifically the intermediate and narrow width Balmer emission lines that are formed due to recombination that follows ionization of CSM material due to shock or radiative heating. It has been suggested (Smith et al. 2007, 2010) that the intermediate-width emission lines are formed within the shocked CSM and thus are related to the velocity of the forward shock, while the narrow-width components are formed in the mediated but yet un-shocked, extended CSM material. In contrast, SN 2008es developed only intermediate-width hydrogen emission lines while narrow-width components were not detected (Gezari et al. 2009; Miller et al. 2009). The lack of narrow-width emission could be due to a variety of reasons. One could be that the ionizing radiation from the forward (and maybe the reverse) shock while it was in the dense shell was not strong enough to ionize dilute material beyond the CSM shell. Another idea is that the interaction was dominated by a fast-moving CSM shell that only gave rise to intermediate-width emission lines, and that an extended CSM was either absent or of too low density to have an effect on the observed spectrum. Emission due to CSM interaction may produce a blue continuum even in a hydrogen and helium deficient CSM (A. Gal-Yam 2013, private communication). The late-time (+414 days) spectrum of SN 2007bi does not show a clear blue continuum, but at such late times it is possible that the forward shock has already exited the optically thick CSM shell and is propagating in CSM too dilute to produce observable spectral features.

We thus argue that the absence of narrow line emission or well-defined blue continua in the optical spectra of SLSN does not necessarily constitute an argument against CSM interaction. Following this line of thought, we consider the possibility that

at least some members of the SLSN-I class are powered by H-poor CSM interaction. In such case, one might still expect the appearance of emission lines indicative of an H-poor CSM composition in the spectra of some SLSN-I. A possible example of such intermediate-width emission arising in an H-poor CSM shell could be the [O I] $\lambda\lambda 6300, 6364$ and O I $\lambda 7775$ features in the +54 day and +414 day post-maximum spectra of SN 2007bi (Gal-Yam et al. 2009). Until detailed, non-LTE radiation hydrodynamics models of H-poor CSM interaction models become available, the nature of these lines and their formation sites (either SN ejecta or H-poor CSM) remain debatable. Given these uncertainties, we elect to investigate models of CSM interaction even for SLSN-I events (see Chatzopoulos & Wheeler 2012, for a formation scenario for H-poor CSM shells).

A simplified version of CSM interaction is the TH model that assumes constant shock energy deposition in the SN ejecta, E_{sh} , for a timescale t_{sh} . The fitting results for the TH models are presented in Table 5. The derived E_{sh} values for all SLSNe in our sample range from 0.5 to 2×10^{51} erg, typical of SN radiated energies ($\sim 10^{51}$ erg) with the exception of CSS100217, which is an outlier for all models. We suspect that the reason for that is the combination of high peak luminosity and very slow LC evolution, which requires both large energy input that is efficiently converted to radiation and large diffusion mass. In most cases, the derived t_{sh} is strongly correlated with t_{rise} and sets the characteristic LC timescale and the total mass of the optically thick SN ejecta and CSM that is heated by the constant energy shock, $M_{CSM,th}$. Due to their unprecedented, long-duration LCs, SN 2008iy and CSS100217 imply extraordinary values for $M_{CSM,th}$. All other events yield values that can be representative of SNe surrounded by dense shells or optically thick winds ($M_{CSM,th} \sim 2\text{--}15 M_{\odot}$ accounting for the uncertainty due to κ , especially in the case of SLSN-I). The TH model fitting parameters are not as tightly correlated as those of the other LC models discussed here (see the [Appendix](#)).

The CSM+RD model is a more detailed version of the CSM interaction model that is described in Section 2 and by Chatzopoulos et al. (2012). This model also includes contributions from the radioactive decays of ^{56}Ni and ^{56}Co . The CSM+RD model fitting parameters for the H-rich events are presented in Table 6, while those for the H-poor events are given in Table 7. In all of our fits, we fixed the slope of the inner SN ejecta density profile to be $\delta = 2$ and that of the outer SN ejecta to be $n = 12$. We fixed the slope of the CSM density profile to be $s = 0$, indicative of a constant density CSM shell, but we also investigated cases of $s = 2$ characteristic of r^{-2} steady-state winds to determine what type of CSM environment is more relevant to SLSNe.

We find that all SLSNe, of both types, can be well fitted by CSM+RD models. Most SLSN LCs are fit better under the assumption of constant density ($s = 0$), relatively massive CSM shells. The derived M_{CSM} values for SLSN-II range from ~ 3 to $5 M_{\odot}$, with the exception of CSS100217, which yields an extraordinary $\sim 77 M_{\odot}$. For SLSN-I, the derived M_{CSM} range is shifted to somewhat smaller values ($\sim 1\text{--}4 M_{\odot}$). This may be consistent with the less massive H-poor shells that are expected to be ejected from more compact progenitors which have lost their large hydrogen envelopes (Chatzopoulos & Wheeler 2012). The derived SN energies and ejecta masses span the whole range between typical and energetic CCSNe ($10^{51} \text{ erg} < E_{SN} < 10^{52} \text{ erg}$; $7 M_{\odot} < M_{ej} < 50 M_{\odot}$). Again, CSS100217 is a significant exception. We find typical distances of the CSM shell from the progenitor star ($\sim 10^{15}$ cm). This is naturally expected because

this is the radius at which radiation is most efficiently emitted and why ordinary supernovae have photospheres at 10^{15} cm near maximum light. CSM densities are characteristic of those proposed for LBV or PPISN shells (10^{-12} – 10^{-10} g cm $^{-3}$; Woosley et al. 2007; Smith et al. 2007; van Marle et al. 2010).

The best-fit CSM+RD models also predict extreme mass-loss properties for the progenitors of SLSNe in the years preceding the SN explosion. The derived characteristic R_{CSM} of $\sim 10^{15}$ cm together with fiducial ejected CSM shell speeds of ~ 100 – 1000 km s $^{-1}$ imply that, if CSM interaction is relevant to most SLSNe, the CSM shells associated with it were ejected only a few months up to a few years prior to the SN explosion. A possible mechanism could be mass loss via gravity waves during the advanced burning stages of some massive stars (Quataert & Shiode 2012). Other potential mass-loss mechanisms are LBV-type mass loss reminiscent to η -Carina (Smith et al. 2007), or shell ejection in the context of PPISN (Woosley et al. 2007; Chatzopoulos & Wheeler 2012).

We were unable to recover a good $s = 2$ fit for SN 2006gy ($\chi^2/\text{dof} = 49.3$), in agreement with the results of Moriya et al. (2013). Our results for the $s = 2$ model of PTF 09uj are in good agreement within uncertainties with those of Ofek et al. (2010), who determined that the event could be explained as shock breakout through an optically thick wind with characteristic wind velocity $v_w = 100$ km s $^{-1}$ and mass-loss rate $\dot{M} = 0.1 M_{\odot}$ yr $^{-1}$. Using our best-fitted $\rho_{\text{CSM},1}$ and R_p values, we estimate $\dot{M} = 0.33 M_{\odot}$ yr $^{-1}$ for the same value for v_w . The SLSN-I SN2010gx is also best fit by an $s = 2$ CSM+RD model that implies $\dot{M} = 1.33 M_{\odot}$ yr $^{-1}$ for $v_w = 100$ km s $^{-1}$ (\dot{M} can be scaled down for higher choices for v_w). That result is in agreement with the findings of Ginzburg & Balberg (2012) that a dense CSM wind with $\rho \sim r^{-2}$ can reproduce the LC.

Although the CSM+RD model provides the best and most physically consistent fits to the LCs of SLSNe, it can be argued that this is due to the large number of fitting parameters associated with it. We argue, regardless, that it is relevant to attempt to fit SN LC CSM+RD models because they also capture some of the natural complexity of the CSM interaction phenomenon. We find most of the CSM+RD parameters to be tightly correlated or anticorrelated with each other, with the natural exception of M_{Ni} . In addition, we find that for all best-fit CSM+RD models the additional RD input has a negligible effect on the final output LC even though in some cases large M_{Ni} masses are found.

5. SUMMARY AND CONCLUSIONS

Making use of the capabilities of the new χ^2 -minimization code MINIM, we fit three main semi-analytic SN LC input power models (RD, MAG, CSM+RD) to the observed pseudo-bolometric LCs of a sample of 10 SLSNe (5 SLSN-I and 5 SLSN-II events) and 2 normal luminosity SNe IIn. Our fitting procedure with MINIM allowed for the calculation of fitting parameter uncertainties, correlation, and degeneracy, which helped us assess the quality and physical implications of our fits. We then evaluated our results and determined which models best fit each individual event, taking into account the consistency with other observations such as spectroscopy. The basic aim of this study was to provide insight to the question of the observed diversity of SLSN LCs and to understand if it arises as a result of one dominant mechanism that involves many parameters or by a combination of different power mechanisms. We also test the power of the semi-analytic CSM+RD model that we introduced

in an earlier work (Chatzopoulos et al. 2012) by applying it to the LCs of normal and superluminous Type IIn events. The main results of our study are summarized below:

1. The derived blackbody temperatures of SLSNe at peak luminosity are similar between the two spectroscopic types. Specifically, SLSN-I do not appear to be systematically hotter than SLSN-II.
2. The semi-analytic CSM+RD model can reproduce the available numerical model LCs for SN 2006gy, accounting for the model assumptions and uncertainties.
3. The power of the semi-analytic CSM+RD model is that it can be easily fit to observed SN LCs and be then used as a reference point for more detailed radiation hydrodynamics calculations.
4. The lack of observations during the rising part of the LC for a few SLSNe poses a serious problem in determining accurate explosion dates that, in turn, introduces large uncertainties in estimates of ejecta mass. The LCs of SN 2006tf and SN 2010kd, but maybe also SN 2007bi, are examples of this issue.
5. The LCs of the majority of SLSNe cannot be powered solely by the radioactive decays of ^{56}Ni and ^{56}Co (RD model) because the ^{56}Ni mass needed to power their peak luminosities either exceeds or is close to the total SN ejecta mass implied from the duration of the LC, for a reasonable choice of SN ejecta opacities.
6. Models of magnetar spin-down (MAG model) provide reasonable fits to the LCs of most SLSNe, but are more relevant to SLSN-I. A significant uncertainty for the MAG models is the issue of the thermalization of pulsar radiation in the expanding SN ejecta.
7. CSM interaction models provide the best fits to all SN LCs in our sample (see Table 8). These models are certainly relevant to the SLSN-II category where clear signs of H-rich CSM interaction are seen in the spectra and cannot be ruled out for SLSN-I events.
8. In most cases, models of constant density CSM shells ($s = 0$) provide better fits than steady-state winds ($s = 2$) to the LCs of SLSNe. That could mean that the environments around extreme SNe are also extreme, possibly formed via episodic mass loss and shell ejection events.
9. The CSM interaction models imply SN ejecta masses (7 – $50 M_{\odot}$), SN energies ($(1$ – $10) \times 10^{51}$ erg), and CSM masses (1 – $5 M_{\odot}$) that are appropriate for high-mass progenitor stars.
10. The CSM shells around SLSN-I are found to be somewhat less massive than those around SLSN-II.
11. For SN 2007bi a hybrid model of H-poor CSM interaction plus radioactive decay model in which the bulk of the energy is supplied by the interaction provides a decent LC. The lack of narrow emission lines and distinct late-time blue continuum do not necessarily constitute lack of H-poor CSM interaction.
12. The extreme CSM environments and mass-loss rates implied by the CSM interaction models indicate that the progenitors of these events were probably quite massive and exploded via energetic CCSNe. With the exception of CSS100217 the combined M_{ej} and M_{CSM} imply progenitor masses significantly smaller than the mass limits for PISNe. The mass-loss mechanisms for these progenitors remain unknown; however, LBVs, PPISNe, and mass loss via gravity waves are some potential candidates.

13. For all LC models investigated in this work most of the fitting parameters are found to be tightly correlated with each other, and hence strongly degenerate. This usually increases the uncertainties of the best-fit parameters and may cause systematic deviations from the true values, especially in the CSM+RD model, which has the largest number of parameters. Thus, despite the success of the LC models in reproducing the results from numerical simulations, one should interpret the best-fit parameters with caution.
14. The diversity of SLSNe in terms of LCs and composition could be the natural result of the diversity of CSM environments around massive progenitor stars, including CS material that is both H and He deficient.

There is growing evidence for hydrogen-deficient CSM. There are a number of events categorized as Type Ibn, by dint of having no evidence of hydrogen, but narrow emission lines of helium corresponding to a photoionized, slowly moving CSM (Pastorello et al. 2008). The SNe Ibn are clearly He rich, but there may be some configuration in which helium is present but not so strongly excited so that it more difficult to detect directly. Another alternative is that the CSM is deficient in both hydrogen and helium (Chatzopoulos & Wheeler 2012). Possible examples of this are SN 2006oz (Leloudas et al. (2012) and the Pan-STARRS discoveries PS1-10ky and PS1-10awh (Chomiuk et al. 2011), PS1-11bam (Berger et al. 2012), PS1-10afx (Chornock et al. 2013), and PS1-10bjz (Lunnan et al. 2013). In this case, one might expect lines of carbon or oxygen of intermediate or narrow width, but again such line emission may depend on the distribution, motion, and ionization of the CSM. If there is a single physical mechanism that accounts for all SLSNe, then economy of hypotheses argues that it is CSM interaction as strongly indicated for the SLSN-II. Our main result is that SLSN LCs of both types can be reasonably reproduced by CSM+RD models. This raises the importance of accurately modeling the radiation from CSM interaction that involves a variety of geometries and compositions for the CSM.

The suggestion that CSM interaction is the common process could have an impact on the interpretation of some SLSN-I events, especially SN 2007bi, as PISNe. Kasen et al. (2011) explored PISN model spectra for SN 2007bi; however, Dessart et al. (2013) noted that the model spectrum that Kasen et al. compared to the observed one at +51 days after explosion was for a much earlier phase (by ~ 100 days). At later times the model PISN spectra from Kasen et al. will no longer be sufficiently blue, in contradiction with the observations of SN 2007bi. SN 2010kd had spectra rather similar to SN 2007bi (J. Vinko et al., in preparation), but it is very difficult to fit the LC with an RD model because the ^{56}Ni mass must be comparable to or exceed the ejecta mass. This result also casts additional doubt that SN 2007bi must necessarily be a PISN.

If events like SN 2007bi are not PISNe, the most likely alternative is that they result from energetic CCSNe with very massive progenitors. This conclusion is in agreement with the models of Moriya et al. (2010) and Yoshida & Umeda (2011) for SN 2007bi, even though in our models the majority of the input energy is provided by CSM interaction instead of the radioactive decays of ^{56}Ni and ^{56}Co .

One aspect of the CSM+RD model is that by its nature it poses a difficulty in definitively unveiling the characteristics of the progenitor stars. Most of the radiation is produced by CSM interaction and diffused within an optically thick CSM shell that obscures the SN ejecta, at least at early times. In our CSM+RD

parameter study, we find that R_0 and M_{ej} , both parameters relevant to the SN progenitor, are the most weakly constrained.

The large parameter space associated with the CSM+RD model is the natural consequence of the large diversity physically associated with CSM interaction; a variety of combinations of progenitor ($v_{\text{SN}}, R_p, M_{\text{CSM}}$, and n) and CSM ($M_{\text{CSM}}, s, \rho_{\text{CSM},1}$) characteristics can yield a variety of LC shapes, durations, peak luminosities, and decline rates. Different sets of parameters may also yield very similar LCs because of parameter degeneracy. In reality the potential diversity is even larger than implied by the parameters of the CSM+RD model we discuss here; effects of different CSM geometry (bipolar shells, circumstellar disks; Metzger 2010) or clumps (Agnolotto et al. 2009) and composition (H-rich versus H-poor and/or metal-rich) must also play a role. In some ways, just looking at the famous *Hubble* image of η -Carina is itself an illustration of the complexity of CSM environments that can exist around massive evolved stars.

As emphasized here, the extraordinary properties of SLSNe will be probed at a more profound level only via accurate non-LTE radiation hydrodynamical modeling for all different power input mechanisms that will allow for direct comparison not only with observed LCs but also spectra of contemporaneous phases. As recently indicated by the findings of Dessart et al. (2012, 2013), reproducing SLSN LCs alone does not constitute a definitive answer about the nature of a particular event. Understanding of mass-loss mechanisms during the late stages of massive stellar evolution will help unveil how extreme CSM environments are formed around SLSN progenitors and the exact role they play in giving rise to the observed radiative properties of individual SLSNe.

We would like to thank the anonymous referee, Roger Chevalier, Vikram Dwarkadas, Sean Couch, Todd Thompson, and Takashi Moriya for useful discussions and comments. This research is supported by NSF grant AST 11-09801 to J.C.W. E.C. would like to thank the University of Texas Graduate School William C. Powers fellowship for its support of his studies. J.V. is supported by Hungarian OTKA grants K76816 and NN107637.

APPENDIX

FIT PARAMETERS AND PARAMETER CORRELATIONS

In this Appendix we give some details on the fitting of the free parameters of each model and discuss the correlation between parameters as measured by their covariance and correlation matrices. To do so, we first synthesized a generic test LC for each model using the equations given in Section 2. We then ran the code MINIM to independently determine the free parameters and to determine the correlations among them. This also served as a test for the reliability of MINIM and the optimization algorithm we applied (see Section 3). The fitting was successful in all cases, since the initial parameters were recovered within the uncertainties.

A.1. Radioactive Diffusion (RD) Model

First introduced by A80 and A82, this model assumes a spherical, homologously expanding ejecta. The energy input generated by the decay of radioactive ^{56}Ni and ^{56}Co slowly diffuses out from the center to the surface. The resulting LC is expressed as Equation (1) in Section 2, where the meaning of the symbols is also explained. We take advantage of having $vt_d \gg R_0$ for the SNe we consider; thus, the terms involving

Table 9
Model Parameters and Correlation Coefficients for the RD Model

	t_{exp}	M_{Ni}	t_d	A_γ
Initial	0.0	10.0	60.0	300.0
Recovered	0.0	10.0	60.0	300.0
	(0.17)	(0.04)	(0.32)	(3.11)
t_{exp}	1.00	-0.67	-0.86	0.17
M_{Ni}		1.00	0.91	-0.74
t_d			1.00	-0.54

Note. 1σ errors are given in parentheses.

Table 10
Same as Table 9 but for the MAG Model

	t_{exp}	R_0	E_p	t_d	t_p	v
Initial	0.0	1.0	2.0	50.0	30.0	40.0
Recovered	0.0	0.47	2.00	49.99	30.07	42.88
	(0.03)	(0.16)	(0.01)	(0.19)	(0.30)	(10.63)
t_{exp}	1.00	-0.47	0.12	-0.03	-0.24	-0.44
R_0		1.00	-0.39	-0.17	0.31	0.33
E_p			1.00	0.91	-0.91	-0.20
t_d				1.00	-0.91	-0.19
t_p					1.00	0.31

R_0/vt_d can be ignored with respect to t/t_d . This considerably reduces the number of free parameters in this model, resulting in the following:

1. t_{ini} : the initial epoch of explosion, expressed in days relative to a pre-selected fiducial explosion time t_{exp} (see Table 2) for each SN;
2. M_{Ni} : the initial mass of radioactive ^{56}Ni (in M_\odot) synthesized in the explosion;
3. t_d : the effective LC timescale (in days), sometimes termed as diffusion timescale by several authors;
4. A_γ : optical depth of the SN ejecta to gamma-rays, measured at +10 days after explosion.

Figure 5 shows the distribution of random choices of free parameters around the χ^2 minimum for four particular parameter combinations. The general shape of this distribution illustrates the correlation between the two particular parameters: a nearly symmetric distribution means less correlation (parameters are independent), while an elongated shape indicates that these parameters are correlated. In the latter case, if the two parameters are slightly changed according to the direction indicated by the curvature of the χ^2 hypersurface, the output LC remains almost the same. In other words, these parameters cannot be fully recovered in every case; only their linear combination can be determined by the fitting of the LC. Figure 5 suggests that none of the parameters of the RD model are independent (as also implied by the physics of the model); they are more or less correlated with each other. We estimated the correlation between them for each parameter combination by calculating

$$R_{i,j} = \frac{\sum_{k=1}^{N_r} (p_i(k) - p_i(\text{min})) \cdot (p_j(k) - p_j(\text{min}))}{(N_p - 1)\sigma_i\sigma_j}, \quad (\text{A1})$$

where $N_r = 200$ is the number of random vectors (parameter sets) used in MINIM, N_p is the number of free parameters in the particular model, $p_i(k)$ is the i th parameter in the k th vector, $p_i(\text{min})$ is the i th parameter in the parameter vector corresponding to the minimum of the χ^2 , and σ_i is the standard

Table 11
Same as Table 9 but for the TH Model

	t_{exp}	E_{sh}	t_{sh}	t_0
Initial	0.0	1.0	30.0	40.0
Recovered	0.00	1.00	30.00	40.00
	(0.04)	(0.001)	(0.07)	(0.08)
t_{exp}	1.00	-0.19	-0.79	0.17
E_{sh}		1.00	-0.09	0.60
t_{sh}			1.00	-0.50

deviation of the i th parameter around $p_i(\text{min})$. The correlation coefficients can be found in Table 9.

Both Figure 5 and Table 9 show that the correlation between each pair of the physical parameters (M_{Ni} , t_d , and A_γ) is stronger than 50%. The $\sim 90\%$ correlation between M_{Ni} and t_d is known as the ‘‘Arnett-rule’’: at LC peak the input and output power is the same, for example, if the peak occurs later (t_d is longer), then a given peak luminosity needs more initial M_{Ni} .

A.2. Magnetar (MAG) Model

Equation (2) describes the resulting LC when the power input is due to the spin-down of a rapidly rotating magnetar (magnetized neutron star) in the center of the SN ejecta. As explained in Section 2, we have optimized the following LC parameters:

1. t_{ini} : the initial epoch of explosion (in days)
2. R_0 : the radius of the progenitor (in 10^{13} cm)
3. E_p : the initial rotational energy of the magnetar (in 10^{51} erg)
4. t_d : the effective LC timescale, as in the RD model (in days)
5. t_p : the spin-down timescale of the magnetar (in days)
6. v : the expansion velocity of the SN ejecta (in 10^3 km s^{-1}).

The model parameters applied for a test LC and their correlation coefficients are collected in Table 10. Figure 6 displays the distribution of the random vectors in the vicinity of the χ^2 minimum.

As expected, R_0 and v are only weakly constrained parameters, since the LC is not sensitive to their combination of R_0/vt_d appearing in Equation (2), the same as in the case of the RD model. All other parameters could be well recovered, despite the strong correlations between E_p , t_p , and t_d .

A.3. CSM Shell with Top-hat Energy Input (TH) Model

The third model consists of the simple configuration of a thick CSM shell around the SN in which the power input is constant for a certain amount of time and then switches off. The observed LC is governed by the diffusion of thermalized photons to the photosphere that is fixed at the outer radius of the shell. This toy model has the following free parameters:

1. t_{ini} : the initial epoch of explosion (in days)
2. E_{sh} : the total input energy (in 10^{51} erg)
3. t_{sh} : the time interval for the constant energy input (in days)
4. t_0 : the diffusion time in the CSM shell having a fixed photosphere.

Table 11 lists all the parameters of the test model and their correlation coefficients, while in Figure 7 the χ^2 function around the minimum is mapped.

This model has the advantage of having relatively few parameters, and they are less strongly correlated than those of the other models. More specifically, t_{sh} seems to be correlated with t_{rise} but not t_d . Its drawback is, of course, the less physical reality of its assumptions.

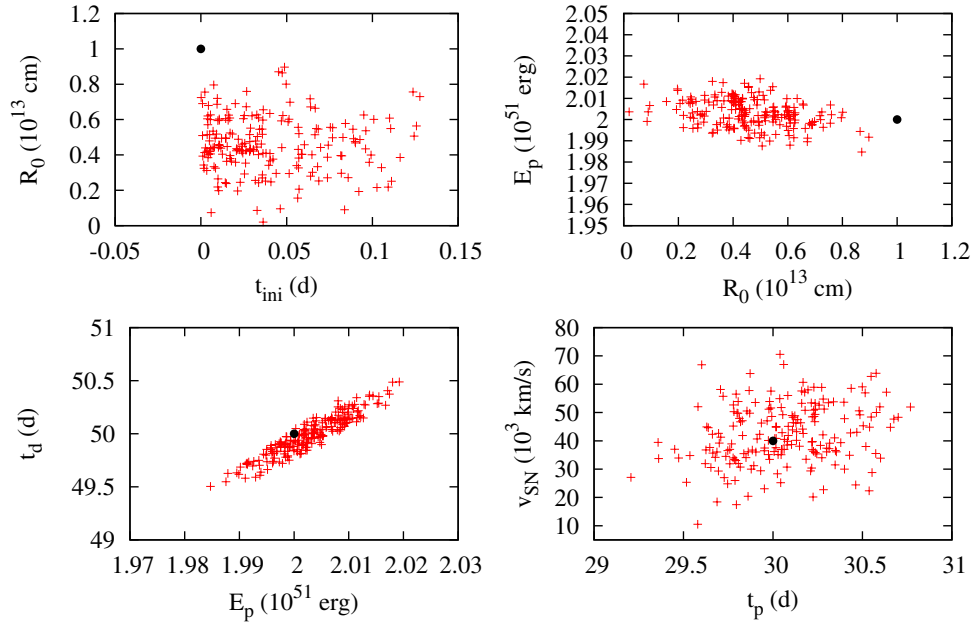


Figure 6. The same as in Figure 5, but for the MAG model. Note that R_0 is especially ill-constrained. For the definition of the fitting parameters plotted here please see Appendix A.2.

(A color version of this figure is available in the online journal.)

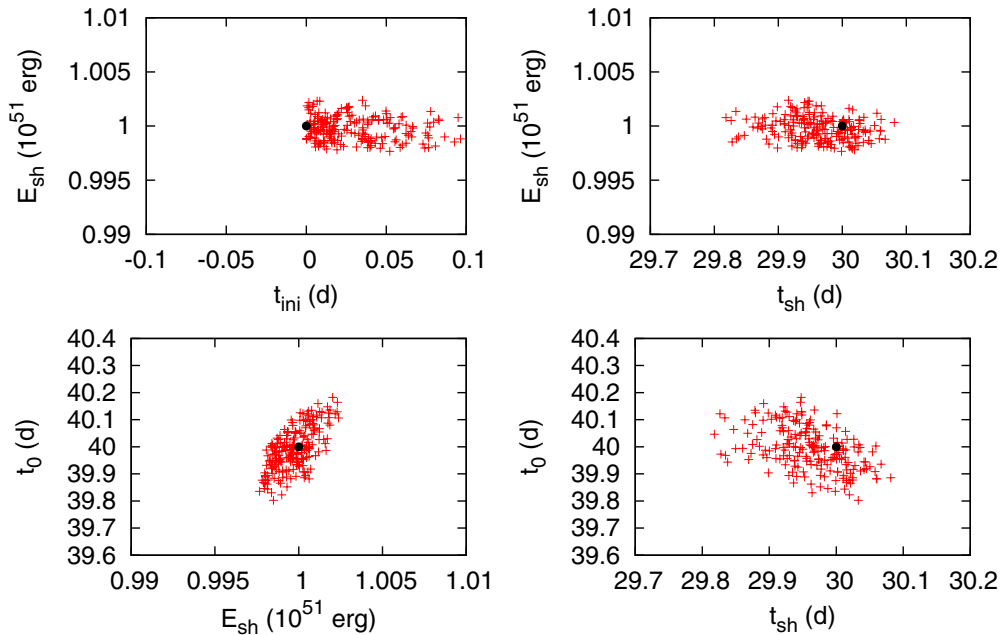


Figure 7. The same as in Figure 5, but for the TH model. For the definition of the fitting parameters plotted here please see Appendix A.3.

(A color version of this figure is available in the online journal.)

A.4. Shock-heated Ejecta and CSM-collision Combined with Radioactive Heating (CSM+RD) Model

This is the most complicated model, where the output LC can be calculated from Equations (4), (5), and (6) (see Section 2 for the details). The large number of parameters makes this model rather ill-constrained. In order to keep the model manageable, we have restricted the number of free parameters to 7:

1. t_{ini} : as before (in days)
2. R_p : radius of the SN progenitor prior to explosion
3. M_{ej} : ejecta mass (in M_{\odot})
4. M_{CSM} : total mass of the CSM (in M_{\odot})

5. $\rho_{\text{CSM},1}$: density of the CSM at radius $R = R_p$ (in $10^{-12} \text{ g cm}^{-3}$)
6. M_{Ni} : initial mass of ^{56}Ni (in M_{\odot})
7. v_{SN} : maximum expansion velocity of the SN ejecta (in 10^3 km s^{-1}).

We elected to use v_{SN} as a free parameter describing the SN kinetic energy via $E_{\text{SN}} = 3/10 \times (n-3)/(n-5) \times M_{\text{ej}}(x_0 v_{\text{SN}})^2$, where n is the ejecta density slope parameter and x_0 is the fractional radius of the core in the SN ejecta (see Section 2).

The remaining parameters were kept fixed to their pre-selected fiducial value: we have applied $\kappa = 0.33 \text{ cm}^2 \text{ g}^{-1}$, $n = 12$, $\delta = 2$, $\beta = 13.8$, $x_0 = 0.1$, and $s = 0, 2$ (see Section 2

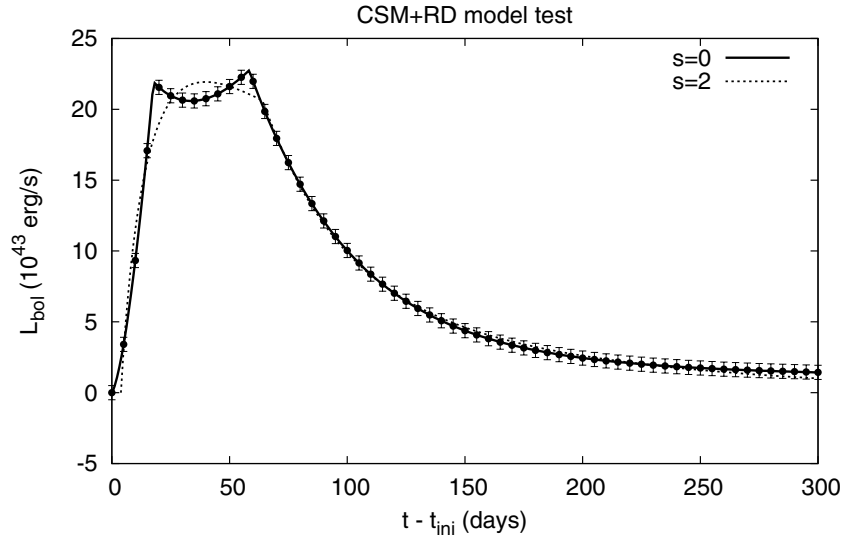


Figure 8. Comparison of CSM+RD models having different density exponents $s = 0$ (constant density CSM) and $s = 2$ (wind-like CSM). The dotted curve represents the initial synthetic model computed assuming $s = 0$ (see Table 12). The solid curve shows the best-fit $s = 0$ model found by MINIM. As seen in Table 12, the parameters of the initial model are recovered very well. Dotted curve shows the best-fit $s = 2$ model. Although the shapes of the LCs are similar, the parameters are quite different in the latter case (Table 12).

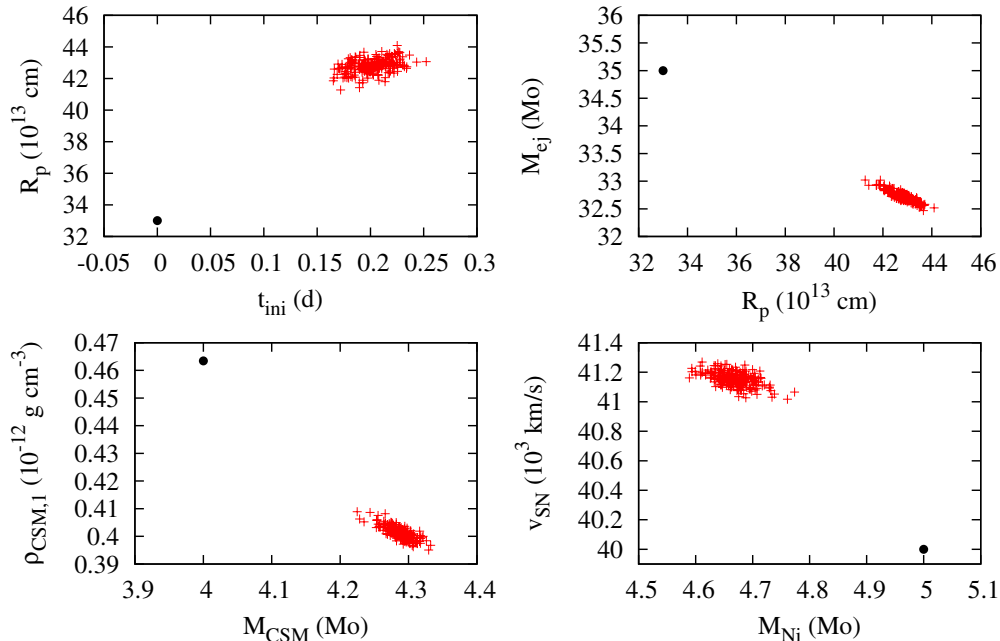


Figure 9. The same as in Figure 5, but for the CSM+RD model assuming $s = 0$ for both the synthetic light curve and the fit model. For the definition of the fitting parameters plotted here please see Appendix A.4.

(A color version of this figure is available in the online journal.)

for explanation). Our tests showed that the LC is not particularly sensitive to these parameters, except for the CSM density slope parameter, s , where the $s = 0$ (constant CSM density) and the $s = 2$ (stellar wind with constant mass-loss rate) assumptions resulted in quite different LCs.

As a test case we have computed a model by assuming $s = 0$, which was then refitted using MINIM with both $s = 0$ and $s = 2$ (s was kept fixed during the fitting). Figure 8 shows the original model LC (dots) and the fit results (solid and dotted lines). It is seen that the shape of the LC can be recovered quite well. The original and recovered parameters (Table 12; Figure 9), however, reveal larger differences than for the previous three models.

Given the larger number of free parameters and the complicated nature of this model, it is not surprising that the correlation between most parameters is quite high. Moreover, there is a general ambiguity related to the choice of the CSM density parameter s . As seen in Table 12 and Figure 9, the resulting fit parameters assuming $s = 2$ can be quite off from the original ones computed assuming $s = 0$. R_0 and M_{ej} are the most weakly constrained parameters, as there are order-of-magnitude differences between their original and reconstructed values for $s = 2$. The other parameters can be recovered within a factor of 2–3. Higher uncertainties for R_0 and M_{ej} are also seen even using the original value of $s = 0$ during the fitting. Thus, it is concluded that even though the shape of the LC can be

Table 12
Model Parameters and Correlation Coefficients for the CSM+RD Model

	t_{exp}	R_0	M_{ej}	M_{CSM}	\dot{M}	M_{Ni}	v_{SN}
Initial	0.0	33.0	35.0	4.0	0.01	5.0	40.0
Recovered $s = 0$	0.20 (0.02)	42.80 (0.44)	32.72 (0.09)	4.29 (0.02)	0.40 (0.01)	4.67 (0.03)	41.15 (0.05)
t_{exp}	1.00	0.40	-0.35	0.06	-0.21	0.06	0.51
R_0		1.00	-0.90	0.73	-0.89	-0.58	0.97
M_{ej}			1.00	-0.69	0.87	0.54	-0.89
M_{CSM}				1.00	-0.80	-0.88	0.68
\dot{M}					1.00	0.63	-0.86
M_{Ni}						1.00	-0.54
Recovered $s = 2$	3.85 (0.07)	17.23 (1.69)	1.11 (0.07)	4.68 (0.04)	10.33 (2.08)	6.90 (0.06)	40.00 (0.13)
t_{exp}	1.00	-0.62	0.44	-0.84	0.63	0.01	-0.40
R_0		1.00	-0.42	0.80	-0.98	0.10	0.21
M_{ej}			1.00	-0.57	0.45	-0.63	-0.86
M_{CSM}				1.00	-0.79	0.06	0.54
\dot{M}					1.00	-0.15	-0.23
M_{Ni}						1.00	0.25

relatively well described by the CSM+RD model either assuming constant density ($s = 0$) or wind-like ($s = 2$) CSM structure, the resulting fit parameters for the SN ejecta (R_0 and M_{ej}) may be off by an order of magnitude from their real values because of the incorrect assumed value of s . The CSM-related parameters (M_{CSM} and $\rho_{\text{CSM},1}$) might be recovered with slightly better accuracy, but those are still only weakly constrained.

REFERENCES

- Agnoletto, I., Benetti, S., Cappellaro, E., et al. 2009, *ApJ*, 691, 1348
- Aldering, G. S., Antilogus, P., Aragon, C., et al. 2009, *BAAS*, 41, 401
- Arnett, W. D. 1980, *ApJ*, 237, 541
- Arnett, W. D. 1982, *ApJ*, 253, 785
- Arnett, W. D., & Fu, A. 1989, *ApJ*, 340, 396
- Barbary, K., Dawson, K. S., Tokita, K., et al. 2009, *ApJ*, 690, 1358
- Berger, E., Chornock, R., Lunnan, R., et al. 2012, *ApJL*, 755, L29
- Blinnikov, S. I., & Bartunov, O. S. 1993, *A&A*, 273, 106
- Brachetti, P., de Felice Ciccoli, M., di Pillo, G., & Lucidi, S. 1997, *J. Glob. Optim.*, 10, 165
- Bucciantini, N., Thompson, T. A., Arons, J., Quataert, E., & Del Zanna, L. 2006, *MNRAS*, 368, 1717
- Chatzopoulos, E., & Wheeler, J. C. 2012, *ApJ*, 748, 42
- Chatzopoulos, E., Wheeler, J. C., & Vinko, J. 2009, *ApJ*, 704, 1251
- Chatzopoulos, E., Wheeler, J. C., & Vinko, J. 2012, *ApJ*, 746, 121
- Chatzopoulos, E., Wheeler, J. C., Vinko, J., et al. 2011, *ApJ*, 729, 143
- Chevalier, R. A. 1982, *ApJ*, 258, 790
- Chevalier, R. A. 2013, arXiv:1304.5500
- Chevalier, R. A., & Fransson, C. 1994, *ApJ*, 420, 268
- Chevalier, R. A., & Fransson, C. 2001, arXiv:astro-ph/0110060
- Chevalier, R. A., & Irwin, C. M. 2011, *ApJL*, 729, L6
- Chevalier, R. A., & Irwin, C. M. 2012, *ApJL*, 747, L17
- Chevalier, R. A., & Soker, N. 1989, *ApJ*, 341, 867
- Chomiuk, L., Chornock, R., Soderberg, A. M., et al. 2011, *ApJ*, 743, 114
- Chornock, R., Berger, E., Rest, A., et al. 2013, *ApJ*, 767, 162
- Chugai, N. N., Blinnikov, S. I., Cumming, R. J., et al. 2004, *MNRAS*, 352, 1213
- Chugai, N. N., & Danziger, I. J. 1994, *MNRAS*, 268, 173
- Colgate, S. A., Petschek, A. G., & Kriese, J. T. 1980, *ApJL*, 237, L81
- Dessart, L., Hillier, D. J., Waldman, R., Livne, E., & Blondin, S. 2012, *MNRAS*, 426, L76
- Dessart, L., Waldman, R., Livne, E., Hillier, D. J., & Blondin, S. 2013, *MNRAS*, 428, 3227
- Drake, A. J., Djorgovski, S. G., Mahabal, A. A., et al. 2009, *ATel*, 2087, 1
- Drake, A. J., Djorgovski, S. G., Mahabal, A., et al. 2011, *ApJ*, 735, 106
- Gal-Yam, A. 2012, *Sci*, 337, 927
- Gal-Yam, A., Mazzali, P., Ofek, E. O., et al. 2009, *Natur*, 462, 624
- Gänsicke, B. T., Levan, A. J., Marsh, T. R., & Wheatley, P. J. 2009, *ApJL*, 697, L129
- Gezari, S., Halpern, J. P., Grupe, D., et al. 2009, *ApJ*, 690, 1313
- Ginzburg, S., & Balberg, S. 2012, *ApJ*, 757, 178
- Heger, A., & Woosley, S. E. 2002, *ApJ*, 567, 532
- Kasen, D., & Bildsten, L. 2010, *ApJ*, 717, 245
- Kasen, D., Woosley, S. E., & Heger, A. 2011, *ApJ*, 734, 102
- Leloudas, G., Chatzopoulos, E., Dilday, B., et al. 2012, *A&A*, 541, A129
- Lunnan, R., Chornock, R., Berger, E., et al. 2013, *ApJ*, 771, 97
- Maeda, K., Tanaka, M., Nomoto, K., et al. 2007, *ApJ*, 666, 1069
- Mahabal, A. A., Drake, A. J., Djorgovski, S. G., et al. 2010, *ATel*, 2490, 1
- Metzger, B. D. 2010, *MNRAS*, 409, 284
- Miller, A. A., Chornock, R., Perley, D. A., et al. 2009, *ApJ*, 690, 1303
- Miller, A. A., Silverman, J. M., Butler, N. R., et al. 2010, *MNRAS*, 404, 305
- Moriya, T. J., Blinnikov, S. I., Tominaga, N., et al. 2013, *MNRAS*, 428, 1020
- Moriya, T., Tominaga, N., Blinnikov, S. I., Baklanov, P. V., & Sorokina, E. I. 2011, *MNRAS*, 415, 199
- Moriya, T., Tominaga, N., Tanaka, M., Maeda, K., & Nomoto, K. 2010, *ApJL*, 717, L83
- Nadyozhin, D. K. 1994, *ApJS*, 92, 527
- Ofek, E. O., Fox, D., Cenko, S. B., et al. 2013, *ApJ*, 763, 42
- Ofek, E. O., Rabinak, I., Neill, J. D., et al. 2010, *ApJ*, 724, 1396
- Ostriker, J. P., & Gunn, J. E. 1971, *ApJL*, 164, L95
- Pan, T., Patnaude, D. J., & Loeb, A. 2013, *MNRAS*, 433, 838
- Pastorello, A., Mattila, S., Zampieri, L., et al. 2008, *MNRAS*, 389, 113
- Pastorello, A., Smartt, S. J., Botticella, M. T., et al. 2010, *ApJL*, 724, L16
- Quataert, E., & Shiode, J. 2012, *MNRAS*, 423, L92
- Quimby, R. M., Aldering, G., Wheeler, J. C., et al. 2007, *ApJL*, 668, L99
- Quimby, R. M., Kulkarni, S. R., Kasliwal, M. M., et al. 2011, *Natur*, 474, 487
- Quimby, R. M., Kulkarni, S. R., Ofek, E., et al. 2010, *ATel*, 2492, 1
- Quimby, R. M., Yuan, F., Akerlof, C., & Wheeler, J. C. 2013, *MNRAS*, 431, 912
- Schlegel, D. J., Finkbeiner, D. P., & Davis, M. 1998, *ApJ*, 500, 525
- Smith, N., Chornock, R., Li, W., et al. 2008, *ApJ*, 686, 467
- Smith, N., Chornock, R., Silverman, J. M., Filippenko, A. V., & Foley, R. J. 2010, *ApJ*, 709, 856
- Smith, N., Li, W., Foley, R. J., et al. 2007, *ApJ*, 666, 1116
- Smith, N., & McCray, R. 2007, *ApJL*, 671, L17
- Soker, N., Frankowski, A., & Kashi, A. 2010, *NewA*, 15, 189
- Svirski, G., Nakar, E., & Sari, R. 2012, *ApJ*, 759, 108
- Valenti, S., Benetti, S., Cappellaro, E., et al. 2008, *MNRAS*, 383, 1485
- van Marle, A. J., Smith, N., Owocki, S. P., & van Veelen, B. 2010, *MNRAS*, 407, 2305
- Vinko, J., Zheng, W., Pandey, S. B., et al. 2012, American Astronomical Society Meeting Abstracts, 219, 436.04
- Vinko, J., Zheng, W., Romadan, A., et al. 2010, *CBET*, 2556, 1
- Wood-Vasey, W. M., Wang, L., & Aldering, G. 2004, *ApJ*, 616, 339
- Woosley, S. E. 2010, *ApJL*, 719, L204
- Woosley, S. E., Blinnikov, S., & Heger, A. 2007, *Natur*, 450, 390
- Yoshida, T., & Umeda, H. 2011, *MNRAS*, 412, L78